

Politecnico di Torino

Master course in Automotive Engineering

A.A. 2019/2020



Master's Thesis

Use of CFD3D analysis results for robust thermal model of piston crown

Candidate:

Iacopo Stoppato

Supervisor:

Cristiana Delprete

Tutor:

Alessandra Gallinatti

CONTENTS

LIST OF FIGURES AND TABLES.....	4
NOMENCLATURE	7
SOFTWARES LIST	8
1 INTRODUCTION.....	9
2 THEORY	10
2.1 Heat transfer	10
2.1.1 Thermal conduction.....	10
2.1.2 Thermal convection.....	10
2.1.3 Thermal radiation	10
2.2 Thermal load on piston	11
2.2.1 Heat source and heat balance.....	11
2.2.2 Temperature profile	12
2.3 Steady-state thermal analysis.....	14
2.3.1 Methodology.....	14
2.3.2 FEM analysis.....	14
2.3.3 GT-Power Boundary conditions.....	17
2.3.4 CFD3D Boundary conditions.....	19
3 LITERATURE REVIEW	22
3.1 Empirical and Semi-Empirical Models.....	22
3.1.1 Combustion parameter and piston crown.....	22
3.1.2 Oil Gallery.....	24
3.1.3 Ring-pack and Skirt.....	25
3.1.4 Undercrown.....	27
3.2 INVERSE HEAT CONDUCTION METHOD.....	28
3.3 MEASUREMENTS TECHNIQUE.....	30
3.3.1 Templug	30
3.3.2 Telemetry	31
3.3.3 Templug vs Telemetry.....	31
3.4 LIMIT TEMPERATURE FOR AI ALLOYS	31
4 ACTUAL PROCEDURE ANALYSIS.....	33
4.1 GT-POWER TUNING	33
4.2 CFD3D TUNING	36
5 CROSS-FUNCTIONALITY MEETING.....	40
5.1 CROSS-FUNCTIONALITY MEETING: GT-POWER.....	40
5.2 CROSS-FUNCTIONALITY MEETING: CFD3D	41
5.3 CFD3D & GT-POWER INTERACTION.....	42
6 NEW PROCEDURE PROPOSAL	43
6.1 NEW WORKFLOW	43
6.2 NEW TOOL AND CORRESPONDENT FLOWCHART	46
6.3 PROCEDURE COMPARISON.....	49

7	INLINE 6 CYLINDER AI-ALLOY PISTON CASE STUDY.....	52
7.1	GT-POWER TUNING	53
7.2	CFD3D TUNING: ACTUAL PROCEDURE	55
7.3	NEW TOOL TUNING	57
7.4	FINAL COMPARISON	61
7.5	THERMAL BALANCE ANALYSIS.....	63
8	INLINE 6 CYLINDER STEEL PISTON CASE STUDY	65
8.1	GT-POWER TUNING	67
8.2	CFD3D TUNING: ACTUAL PROCEDURE	69
8.3	NEW TOOL TUNING	71
8.4	FINAL COMPARISON	75
8.5	LOOP CONVERGENCY (ITERATIVE PROCEDURE)	77
9	CONCLUSIONS	78
10	NEXT STEPS	79
	REFERENCES	80
	ACKNOWLEDGMENTS	83

LIST OF FIGURES AND TABLES

Figure 2.1 – Piston heat distribution [2]	11
Table 2.1 – Piston heat distribution for different design [2].....	12
Figure 2.2 – Salt-core cooling gallery geometry [2]	12
Figure 2.3 & 2.4 – Combustion plume (left) & Thermal gradient (right) [2]	13
Figure 2.5 – Temperature distribution in Diesel and gasoline engines [2]	13
Figure 2.6 – Body with boundaries [4]	15
Figure 2.7 – GT-Power engine map model.....	17
Figure 2.8 – GT-Power T, p, HTC traces	18
Figure 2.9 – GT-Power engine simulation workflow	19
Figure 2.10 – Computational domain	20
Figure 2.11 – T, p and HRR traces.....	20
Figure 3.1 – Piston model [4].....	23
Figure 3.2 – Cooling gallery [4].....	25
Figure 3.3 – Ring-pack assembly [4]	26
Figure 3.4 – Thermal circuit method [4].....	27
Figure 3.5 – Piston undercrwon [4].....	27
Figure 3.6 – IHCM flowchart [4].....	29
Figure 3.7 – Fatigue resistance of Al-alloys [2].....	32
Figure 4.1 – Actual procedure workflow	33
Figure 4.2 – GT-Power piston model.....	34
Figure 4.3 – GT-Power tuning thermal map	35
Figure 4.4 – CFD3D HTCs distribution.....	36
Figure 4.5 – CFD3D Tgas distribution	37
Figure 4.6 – CFD3D Qflux distribution.....	37
Figure 4.7 – CFD3D tuning thermal map.....	38
Figure 6.1 – New procedure workflow	46
Figure 6.3 – New tool flowchart legend	47
Figure 6.2 – New flowchart.....	48

Figure 6.4 – Thermal map with new tool and procedure.....	49
Figure 6.5 – Actual procedure	50
Figure 6.6 – New procedure	50
Table 6.1 – Procedure comparison	51
Figure 7.1 – Piston FEM mesh	52
Figure 7.2 – Telemetry sensors.....	52
Table 7.1 – 1 st Loop GTP	53
Table 7.2 – Final Loop GTP	53
Figure 7.3 – Thermal map GTP front.....	54
Figure 7.4 – Thermal map GTP front section	54
Figure 7.5 – Thermal map GTP crown	55
Table 7.3 – CFD3D tuning.....	55
Figure 7.6 – Thermal map CFD3D front	56
Figure 7.7 – Thermal map CFD3D front section.....	56
Figure 7.8 – Thermal map CFD3D crown.....	57
Table 7.4 – CFD3D new tool tuning GTP thermal map	58
Table 7.5 – CFD3D new tool tuning constant T _{wall}	58
Table 7.6 – CFD3D new tool tuning T _{wall} loop 2	59
Figure 7.9 – Thermal map CFD3D new tool front.....	59
Figure 7.10 – Thermal map CFD3D new tool front section.....	60
Figure 7.11 – Thermal map CFD3D new tool crown.....	60
Figure 7.12 – Procedures results comparison	61
Figure 7.13 – T _{wall} sensitivity	62
Figure 7.14 – Final comparison	62
Table 7.7 – Thermal balance analysis.....	63
Figure 8.1 – Piston FEM mesh	65
Table 8.1 – Templugs experimental values	65
Figure 8.2 – CFD3D Qfluxes distribution	66
Table 8.2 – GTP tuning first loop.....	67

Table 8.3 – GTP tuning final loop.....	67
Figure 8.3 – Thermal map GTP front.....	68
Figure 8.4 – Thermal map GTP front section	68
Figure 8.5 – Thermal map GTP crown	69
Table 8.4 – CFD3D actual procedure tuning	69
Figure 8.6 – Thermal map CFD front.....	70
Figure 8.7 – Thermal map CFD front section	70
Figure 8.8 – Thermal map CFD front crown	71
Table 8.5 – CFD3D new procedure tuning constant CFD T _{wall}	72
Table 8.6 – CFD3D new procedure tuning not constant CFD T _{wall}	72
Table 8.7 – CFD3D new procedure tuning constant GTP T _{wall}	73
Table 8.8 – CFD3D new procedure tuning not constant GTP T _{wall}	73
Table 8.9 – CFD3D new procedure tuning T _{wall} from previous loop	74
Figure 8.9 – Thermal map CFD new procedure front.....	74
Figure 8.10 – Thermal map CFD new procedure front section.....	75
Figure 8.11 – Thermal map CFD new procedure crown.....	75
Figure 8.12 – Actual procedure VS New proposal procedure.....	76
Figure 8.13 – T _{wall} choice.....	76
Figure 8.14 – Loop convergency	77

NOMENCLATURE

CFD	Computational Fluid Dynamics
FEM	Finite Element Method
FEA	Finite Element Analysis
HTC	Heat Transfer Coefficient
BC	Boundary Condition
IHCM	Inverse Heat Conduction Method
EGR	Exhaust Gases Recirculation
HRR	Heat Release Rate
SOH	Total Heat Flux
D.O.F.	Degrees of Freedom
G.T.P.	Gamma Technologies Power

SOFTWARES LIST

Hypermesh

Abaqus

AbaqusViewer

MatLab

Visual Studio

Microsoft Office Tools

Internal Operational Tools

1 INTRODUCTION

In recent years the OEM's trend is to develop, especially for Diesel engines, smaller engines with higher specific power outputs to comply with both even more stringent emission requirements and vehicle performance. This leads to higher mechanical and thermal load on all engine components, so it is of fundamental importance to analyze these loads. This thesis work, developed at Punch Torino S.p.a., is focused on the steady-state thermal analysis for Diesel engine pistons, that is the first step of the whole piston design validation process. In particular, the aim was to use results coming from CFD3D analysis as thermal boundary conditions for the FEM simulation to obtain more realistic temperature distributions. To do that the workflow was structured in this way: first was done a deep literature investigation aimed to achieve a greater understanding of the process; after that was analyzed the current procedure used in the company to highlight its strong and weak points and doing in parallel many cross-functionality meeting to examine the robustness of input data. At the end of these steps, considering all acquired information was proposed, a new procedure. For the validation of the new procedure, two different pistons were analyzed, following the actual and the new procedure workflow, to compare and show the main differences between the two and all the possible advantages coming from the new one.

2 THEORY

2.1 Heat transfer

All thermal analyses are focused on the quantification of heat fluxes between systems at different temperatures. The three main heat transfer modes are:

- ❖ Thermal conduction.
- ❖ Thermal convection.
- ❖ Thermal radiation.

All these modes can occur separately or in combination, depending on the considered case.

2.1.1 Thermal conduction

The thermal conduction is the heat transfer mode present in a continuous system with a temperature gradient. The standard equation stated in eq 2.1 is based on the Fourier's Law [1-13]. The heat transfer is calculated considering the thermal gradient ∇T , the area of interest A and a constant k [W/mK] named thermal conductivity.

$$q = -kA\nabla T \quad (2.1)$$

2.1.2 Thermal convection

The thermal convection is the heat transfer mode present along a surface of a body that is in contact with a fluid without mixing. The standard equation stated in eq 2.2. The heat transfer is calculated considering the difference between the surface temperature T_{wall} and the fluid temperature T_{fluid} , the area of interest A and a parameter h [W/m²/K] named heat transfer coefficient related to fluid parameters.

$$q = -hA(T_{wall} - T_{fluid}) \quad (2.2)$$

2.1.3 Thermal radiation

The thermal radiation is the only heat transfer process that does not need of transfer medium. It is characterized by the emission of electromagnetic waves

with different lengths emitted by the surface. The standard equation stated in eq 2.3 express the Stefan Boltzmann's law [1]. The heat transfer is calculated considering the difference between the surface temperatures T_a and T_b , the view factor F , the emission area A , and a constant σ named Stefan-Boltzmann constant.

$$q = F\sigma A(T_a^4 - T_b^4) \quad (2.3)$$

2.2 Thermal load on piston

2.2.1 Heat source and heat balance

It is evident that the thermal load on a Diesel engine piston is cyclic, also if it acts mainly in the expansion stroke, it is present in a minor way in the other phases. The energy stored in the fuel is converted into heat during the combustion, the piston turns a portion of this heat into mechanical work with the help of the conrod-crank system to drive the crankshaft. Exhaust gases dissipate another part of this heat while the last part is transferred through convection and radiation to adjacent components. The heat transfer from hot gases to piston occurs mainly by convection, and a little by radiation. During the expansion stroke, the real combustion thermal load acts for a very short time. However, due to the high thermal inertia of the piston, the temperature distribution is quasi-static. Heat flow in the combustion chamber is entering from the upper part (crown and the first half of the first land), and it is dissipated by all other surfaces, as reported in figure 2.1.

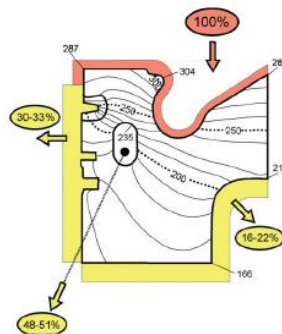


Figure 2.1 – Piston heat distribution [2]

In particular, it has to be highlighted that the two most important ones are the cooling gallery and the ring pack assembly. It is possible to have different cooling types based on various requirements, here below in table 2.1 are typical values of heat flow distribution for different types of pistons. [2]

Piston type	Uncooled piston	Oil-spray cooling	Oil-spray cooling	Salt-core cooling gallery	Cooled ring carrier	MONO-THERM® ring gallery	2-chamber cooling cavity
Operating principle	Gasoline	Gasoline	Diesel	Diesel	Diesel	Diesel	Diesel
Heat flow [%]							
Cooling gallery	0	0	0	40–50	50–60	75–90	90–100
Ring belt	50–60	15–25	50–55	25–45	10–30	0–10	0–5
Skirt	10–15	5–10	10–15	5–10	5–10	0	0
Inner shape	10–20	50–60	20–30	5–15	5–15	0–10	0–5
Window/ undercut	5–10	0–5	0–5	0–5	0–5	0	0
Boss	5–10	0–5	0–15	0–10	0–10	0	0

Table 2.1 – Piston heat distribution for different design [2]

This thesis work is mainly focused on pistons, which present a design choice of the Salt-core cooling gallery type (shown in figure 2.2). As said before, the two most important sources of dissipation are the cooling gallery and the ring-pack.

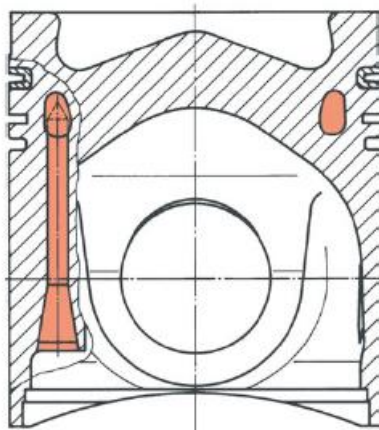


Figure 2.2 – Salt-core cooling gallery geometry [2]

2.2.2 Temperature profile

In gasoline engines, the spark plug triggers the fuel-air mixture, and the combustion starts propagating towards all directions of the combustion chamber in a quite homogeneous way, resulting in a simple and quasi-uniform temperature

distribution. In Diesel engines with direct injection instead, combustion starts close to the injector and propagates in the combustion chamber following the development of the flame front determined by combustion plumes (figure 2.3). The result of this process is a highly heterogeneous temperature distribution, with a high thermal gradient (figure 2.4), especially in the upper part of the piston, so it is of fundamental importance to analyze this process.

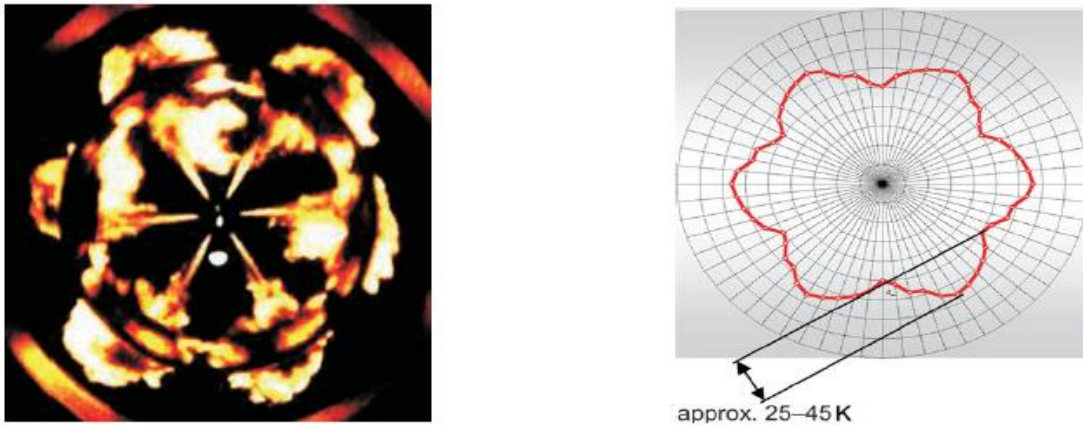


Figure 2.3 & 2.4 – Combustion plume (left) & Thermal gradient (right) [2]

Here below, it is possible to see the differences between Diesel and gasoline engines for what concerns typical temperature distributions.

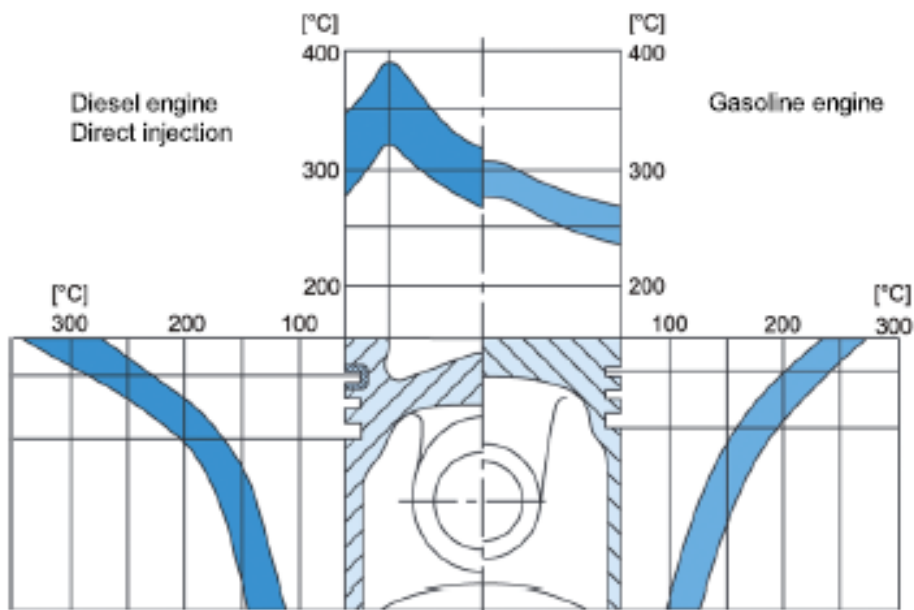


Figure 2.5 – Temperature distribution in Diesel and gasoline engines [2]

2.3 Steady-state thermal analysis

2.3.1 Methodology

The steady-state thermal analysis is the first step of the whole thermo-mechanical fatigue analysis for the validation of a piston design, so being a starting point is of fundamental importance. This process is aimed to derive the thermal map of the piston, a temperature value assigned for each node of the mesh, to be used as boundary conditions in further steps of the procedure. At the present day, the most common technique to do this is the FEM (Finite Element Method), that is supported by other analysis to obtain better boundary conditions.

2.3.2 FEM analysis

The FEM method is a discretization method that divides the whole body into smaller pieces called elements to apply equation relative to the case in exam element by element. Every element has the same physical, geometrical and material properties of the real body; it is composed of nodes and by shape functions that describe the value change along the element; each node has a variable number of degrees of freedom depending on the type of performed analysis. The dimensions of these pieces are so small that it is possible to reduce many simplifications and to reproduce the actual geometry of the examined body. In this thesis work, the software used is Hypermesh as pre-processor, Abaqus as solver, and with AbaqusViewer as post-processor. The following considerations and equations are taken from [4] and based on [3]. The heat transfer analysis is based on equations 2.4 [3]:

$$\begin{aligned} \operatorname{div}(D\nabla T) + Q &= 0 && \text{in } V \\ q^T \mathbf{n} &= q && \text{on } S_q \\ T &= q && \text{on } S_g \\ q &= h(T - T_{amb}) && \text{on } S_c \end{aligned} \tag{2.4}$$

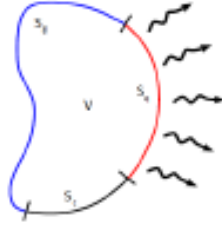


Figure 2.6 – Body with boundaries [4]

In previous equations, D is the constitutive matrix, ∇T is the temperature gradient, Q is the heat, q is the heat flux, n is the normal, T is the temperature, h the convective heat transfer, T_{amb} is the ambient temperature while S are the body boundaries. Multiplying this for a test function v and with the volume integration, it is obtained the weak form as in eq 2.5 and 2.6. [4]

$$\int_V (\nabla v)^T D \nabla T dV = - \int_{S_q} v h dS - \int_{S_g} v q dS + \int_V v Q dV \quad (2.5)$$

$$T = g \text{ on } S_g \quad (2.6)$$

In the thermal analysis, each node has one d.o.f. that is the temperature. The next step is to discretize the body into elements, as in eq 2.7 [4].

$$T = Na \quad (2.7)$$

Where N is the shape function that represents the variation of the temperature value along the element. If the shape function is linear, the elements are first-order, while the quadratic elements are second-order. The conductivity stiffness matrix K shows the heat transfer by conduction into the body. Eq 2.8 defines the stiffness matrix, while eq 2.9 and 2.10 always from [3] define B and the constitutive matrix for isotropic materials D .

$$K = \int_V B^T D B dV \quad (2.8)$$

$$B = \nabla N \quad (2.9)$$

$$D = \begin{bmatrix} k & 0 \\ 0 & k \end{bmatrix} \quad (2.10)$$

In eq 2.11 is expressed the nodal load vector f that is a heat flux. The equation presents the boundary load, the convective heat flow, and the body load [4].

$$f = - \int_S N^T q dS - \int_S N^T h T_{amb} dS + \int_V N^T Q dV \quad (2.11)$$

At this point can be rewritten the weak form in eq 2.12, highlighting the unknown values a that are solved.

$$Ka = f \quad (2.12)$$

The matrix K is modified to take into account the convection, so it is obtained the convective stiffness matrix K_c as in eq 2.13, and in eq 2.14, nodal values are solved. [4]

$$K_c = \int_S h N^T N dS \quad (2.13)$$

$$(K + K_c)a = f \quad (2.14)$$

At this point, remembering the eq 2.2, it is clear that it is necessary to know some of the terms of the equation. These terms, at the end, are the so-called thermal boundary conditions that can be obtained with different approaches. The most common two that will be analyzed in the following chapters are:

- ❖ 1-D fluid-dynamic analysis.
- ❖ CFD3D combustion analysis.

In [5], V. Esfahanian et al. have described a different type of boundary conditions to compare them and find a better trade-off between accuracy and computational cost. In particular they have analyzed three methods for combustion model boundary condition:

1. Surface and cycle-averaged values for gas heat flux at piston crown.
2. Locally cycle-averaged values for gas heat flux at piston crown.
3. Fully locally transient values for gas heat flux at piston crown.

In addition to this, they have also examined three different methods for temperature boundary condition:

1. Time and surface-averaged values of piston crown temperature.
2. Locally time-averaged value of piston crown temperature.
3. Fully locally transient values of piston crown temperature.

The result was also that if the third method leads to more accurate results because it can also consider fluctuations, the use of spatial and time-averaged methods represents the best trade-off.

2.3.3 GT-Power Boundary conditions

The GT-Power model is 1D, and it is composed of the whole powertrain from air filter to exhaust tail. In this type of simulation are considered pressure oscillations and thermal exchange. When they are present, external systems are also considered, such as the Turbo or the EGR. In figure 2.7 is showed a GT-Power map model of the engine.

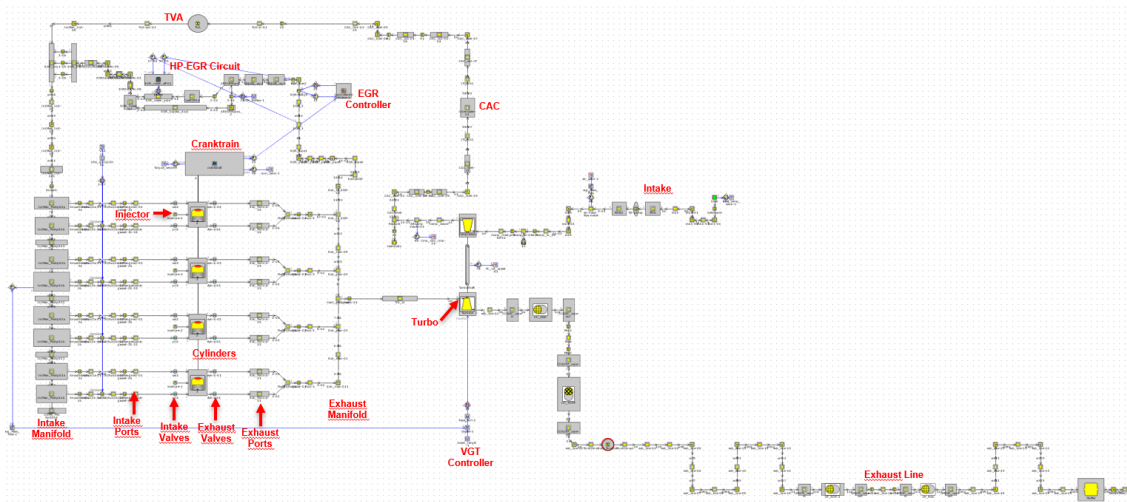


Figure 2.7 – GT-Power engine map model

The combustion model is imposed from experimental data, and so it is not predictive. The input parameters are the following:

- ❖ Internal components simplified geometry.
- ❖ External components reduced to 0D through map.
- ❖ All inlet and exhaust characteristics.

All these parameters are needed to obtain the correct air mass flow rate towards the combustion chamber. After that are considered the compression and combustion phases, the inputs are:

- ❖ FEM model of combustion chamber components.
- ❖ Combustion profile.

The combustion profile is obtained from the pressure cycle at peak power, that is the worst case, and from that are obtained the fuel and the mass airflow rate. From that are obtained pressure and temperatures of gases in 0D and heat fluxes of all the surfaces. In figure 2.8 are showed temperatures, HTC, and heat transfer rate traces from the GT-Power model.

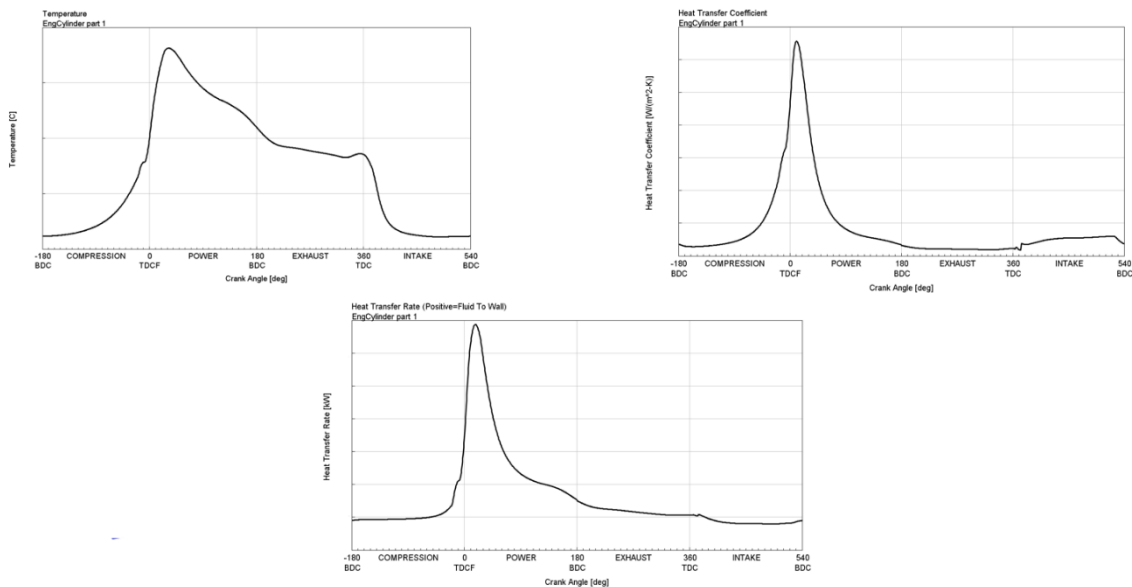


Figure 2.8 – GT-Power T, p, HTCs traces

Once these parameters are known with the formula expressed in eq 2.15 are obtained pistons T_{wall} , HTC, and Q.

$$Q = h_{g,eff} A_{tot} (T_{g,eff} - T_{wall}) \quad (2.15)$$

Here in figure 2.9 is reported an engine simulation workflow.

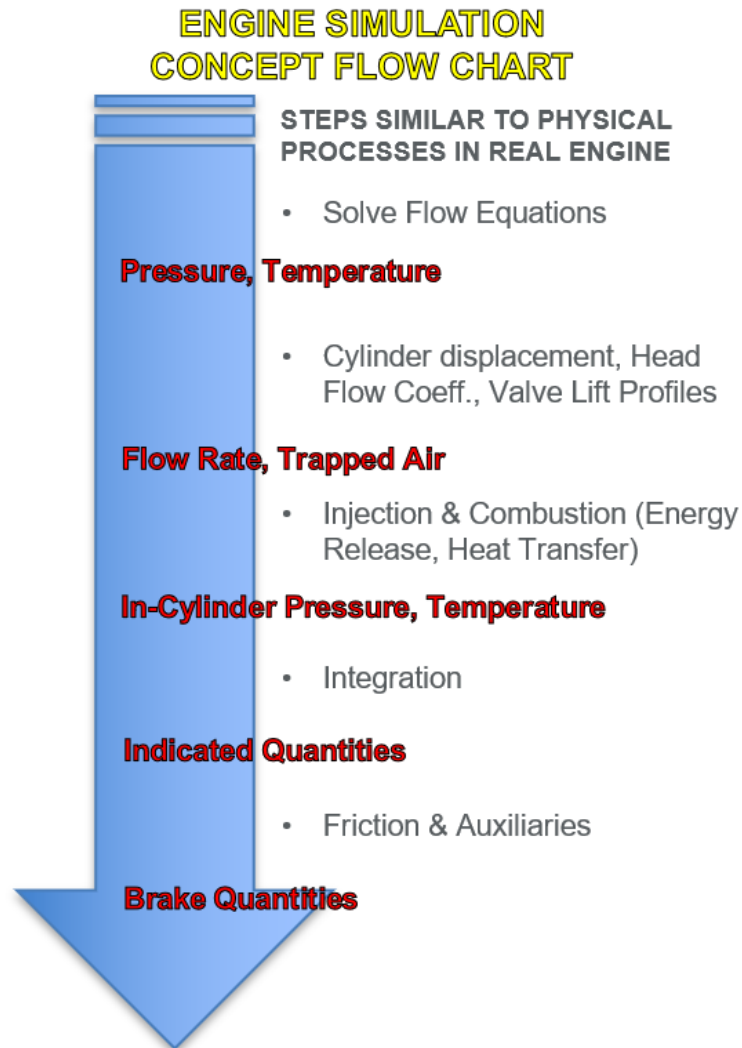


Figure 2.9 – GT-Power engine simulation workflow

2.3.4 CFD3D Boundary conditions

In this chapter are briefly explained the main steps of the CFD3D analysis that leads to the definition for the thermal boundary conditions used in the FEM analysis. This type of analysis is dynamic and 3D. The input parameters are:

- ❖ Pressure and temperature at inlet and the exhaust ducts.
- ❖ Air and fuel mass flow rates.
- ❖ Mean piston speed from cranking mechanism analysis.
- ❖ Wall temperatures of all the surfaces.
- ❖ Computational domain shown in figure 2.10.

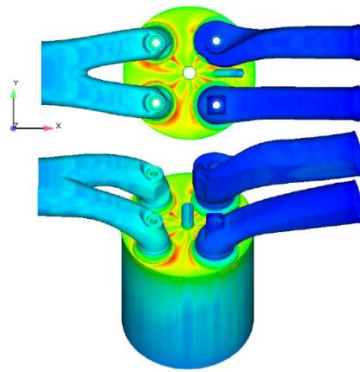


Figure 2.10 – Computational domain

At this point is selected a location in the engine map, and the simulation is done. For what concerns wall temperatures, they can be taken from the previous loop, from GT-Power or imposed as constant value; gas temperature instead is calculated by the software considering: a wall function, a spray model, and a turbulence model, chemical models, and combustion parameters. The outputs of the analysis are:

- ❖ T, p, and HRR traces to be compared with GT-Power ones (figure 2.11).
- ❖ Emissions.
- ❖ Qflux cycle-averaged [W/m²] for each element of the computational domain. (figure 2.10)

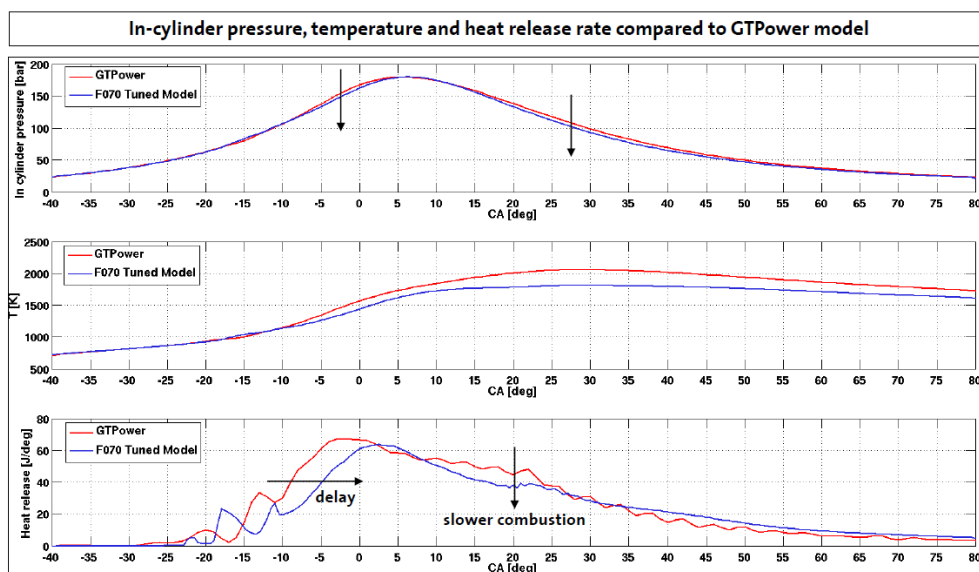


Figure 2.11 – T, p and HRR traces

For what concerns piston thermal boundary conditions, the next step is done with the conduction-convection approximation describe here below in eq 2.16:

$$q = k \frac{T_i - T_w}{\partial x} = h(T_\infty - T_w) \quad (2.16)$$

Where T_i is the gas cycle-averaged temperatures of the closest cell to the surface, T_w is the wall temperature defined as explained before, ∂x is the normal distance of the cell with respect the surface, h is the heat transfer coefficient, and T_∞ is the gas temperature defined with the process described here below in eq 2.17 and 2.18.

$$Q = \sum_i^{CA} h_i / \Delta CA \left(\frac{\sum_i^{CA} h_i * T_{gi} / \Delta CA}{\sum_i^{CA} h_i / \Delta CA} \right) - T_w \quad (2.17)$$

$$Q = \bar{h}(\bar{T}_g - T_w) \quad (2.18)$$

3 LITERATURE REVIEW

A deep literature investigation was performed to obtain a greater understanding of the phenomena and all other related aspects. The research was carried out considering five different search field:

- ❖ Empirical and semi-empirical models.
- ❖ Inverse Heat Conduction Method.
- ❖ Measurements technique.
- ❖ Limit temperature for Al-Alloys.

3.1 Empirical and Semi-Empirical Models

The first part of the literature investigation was mainly focused on all the empirical or semi-empirical methods that could be used to obtain thermal boundary conditions as showed in [6] by Zheng Q. P. et al. It has to be said that these methods, being empirical and semi-empirical, couldn't have a higher accuracy in all cases and situations but could be very useful in an early project phase as a starting point.

The research was divided into four sections:

- ❖ Combustion parameter and piston crown.
- ❖ Oil gallery.
- ❖ Ring-pack assembly and skirt.
- ❖ Undercrown.

3.1.1 Combustion parameter and piston crown

Empirical and semi-empirical formulations treated in this chapter are related to the combustion parameter; they are used to describe the heat transfer in the combustion chamber during gas exchange and for Diesel engines, with a particular focus also on the piston crown.

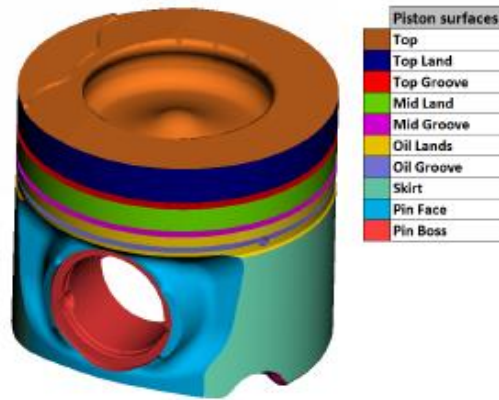


Figure 3.1 – Piston model [4]

In [7] Lu Y. et al. have used a modified Seal-Taylor empirical formula to determine the HTC on the piston top in radial direction as follows:

$$r < N, \quad \alpha_r = \frac{2.2\alpha_m}{\left(1 + e^{0.1\left(\frac{N}{25.4}\right)^{1.9}}\right)} e^{0.1\left(\frac{r}{25.4}\right)^{1.9}} \quad (3.1)$$

$$r > N, \quad \alpha_r = \frac{2.2\alpha_m}{\left(1 + e^{0.1\left(\frac{N}{25.4}\right)^{1.9}}\right)} e^{0.1\left(\frac{(2N-r)}{25.4}\right)^{1.9}} + 0.05\alpha_m \left[\frac{(r-N)}{25.4}\right]^{1.5/1.9} \quad (3.2)$$

N is the distance from the point where the maximum temperature is derived according to the Seal-Taylor experiment, while r is the radial distance to the piston center. The standard correlation developed by Seal and Taylor is instead presented in [13]. Another standard method is to use the Woschni correlation, which is used in particular to estimate the HTC related to the gas exchange process. This approach is used in many technical papers, such as [4] and [8]-[12] and is based on eq 3.3 here below:

$$h_a = \alpha d^{-0.2} p(t)^{0.8} T(t)^{-0.53} \left[C_1 c_m + C_2 \frac{V_s T_1}{p_1 V_1} (p(t) - p_0) \right]^{0.8} \quad (3.3)$$

Where h is the instantaneous area-averaged HTC of the piston crown, α is a constant based on engine geometry, d is the bore, p the pressure, T the gas temperature, c_m the mean piston velocity, V_s the cylinder volume and C_1 - C_2 are two constants based on the considered point of the working cycle. Integrating this expression over the whole cycle, and averaged HTC can be obtained. Another

method very similar to this for combustion parameters is the one proposed by Honenberg and found in [4]. It gives a better correlation for different engine cycles and is based on eq. 3.4:

$$h = C_1 V_c^{-0.06} p^{0.8} T^{-0.4} (v_p + C_2)^{0.8} \quad (3.4)$$

The last two correlations found in the literature are the ones developed by Annad and Ma, and the Eichelberg one. Annad and Ma correlation found in [4] and [12] is aimed to obtain an instantaneous HTC and is described by eq 3.5:

$$h = \left(\frac{k}{D}\right) Re^{0.7} \left(0.12 - 0.2 \frac{dT_g}{dt} \frac{1}{\omega} \frac{1}{T_g - T_\omega}\right) \quad (3.5)$$

D is the bore, k the thermal conductivity of the fluid, ω the angular rotational speed of the crankshaft, Re the Reynolds number, T_g the fluid temperature, and T_ω the wall temperature. The last correlation found in the investigation for what concern piston crown and combustion parameter is the Eichelberg one found in [10],[14] and [15] and is reported in eq 3.6:

$$\alpha_g = K_0 \sqrt[3]{C_m} \sqrt{p_g T_g} \quad (3.6)$$

Where K_0 is a correction coefficient, C_m the mean piston speed, p and T are the gas pressure and temperature. It is clear that these are only a small part of used correlations but are commonly used for Diesel applications.

3.1.2 Oil Gallery

The piston is subjected to high thermal loads, so it needs to be cooled down to avoid damages coming from too high temperatures. In Diesel engines, the main factor that reduces piston's temperatures is the cooling gallery responsible for 50% of dissipated heat, so it is evident that the heat transfer process has to be analyzed carefully.

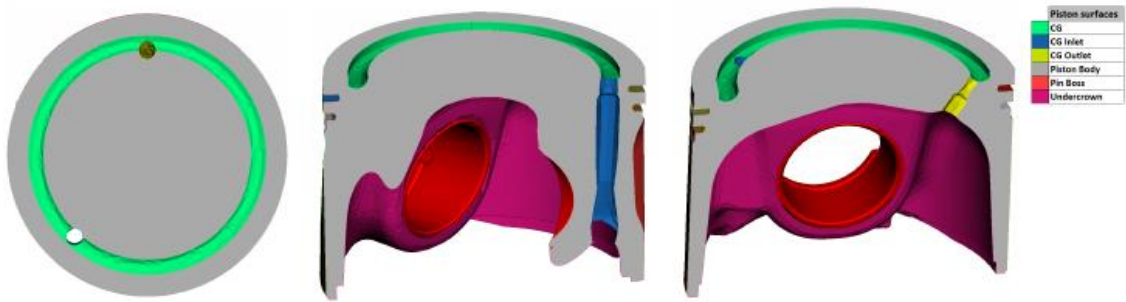


Figure 3.2 – Cooling gallery [4]

For what concerns empirical correlations, the most used two are the ones developed by Bush and by French [4],[7],[9]. The Bush formulas expressed in eq 3.7 and eq 3.8 calculates an area-averaged Nusselt number related to the HTC of the cooling gallery; Bush correlation assumes a different form depending on the value of the Prandtl number as reported here below:

$$\text{For } P_r > 0.5 \quad N_{Bush} = 0.495 Re^{0.57} (D_c)^{0.24} (P_r)^{0.29} \quad (3.7)$$

$$\text{For } P_r \ll 1 \quad N_{Bush} = 0.638 (Re P_r)^{0.5} (D_c)^{0.24} \quad (3.8)$$

Re is the Reynolds number, Pr the Prandtl number, and Dc the diameter of the cooling gallery. After that the HTC is obtained with the eq 3.9, taking into account the fluid thermal conductivity k:

$$h = k N_{Bush} \quad (3.9)$$

The second correlation is a modified version of the previous one and was developed by French and reported in eq 3.10:

$$N_{French} = Re^{0.54} P_r^{\frac{1}{3}} (D/H)^{1/3} (\mu_{in}/\mu_{out})^{0.14} \quad (3.10)$$

Where μ are the dynamic viscosities at the inlet and at the outlet of the cooling gallery, D is the diameter of the gallery while H is the length of the cavity.

3.1.3 Ring-pack and Skirt

The ring-pack assembly is the second contribution to the heat dissipation of piston. It is composed of ring grooves in which are installed the rings (generally three) and by the lands. These rings have three main functions: to guide the

piston motion into the cylinder, to dissipate heat through contact with the lubricated liner surface, to seal and divide the combustion chamber from the crankcase. Due to the higher number of circumstances that can affect the heat flow in this zone is difficult to develop an analytical model. However, as the first assumption due to the small clearance, it can be assumed that the heat transfer is of conduction type between rings and liner.



Figure 3.3 – Ring-pack assembly [4]

In [4], M. Gonera and O. Sadin describe the thermal circuit method that is frequently used to describe the phenomenon. This method is based on an analogy to the electrical circuit. First is evaluated the thermal resistance with eq 3.11:

$$R = L/kA \quad (3.11)$$

Where L is the length of the heat transfer, k the thermal conductivity, and A the area of interest. The same reasoning but with different formulas is done for all the other regions of the ring-pack assembly, and, once it is obtained the total resistance, using the eq 3.12, is derived the relative HTC.

$$h = \frac{1}{R_{tot}A_{ring,groove}} \quad (3.12)$$

This method can also be used with the same reasoning on the skirt, just changing the parameters of the equations and the scheme. Here below in figure 3.4 is reported an example taken from [4].

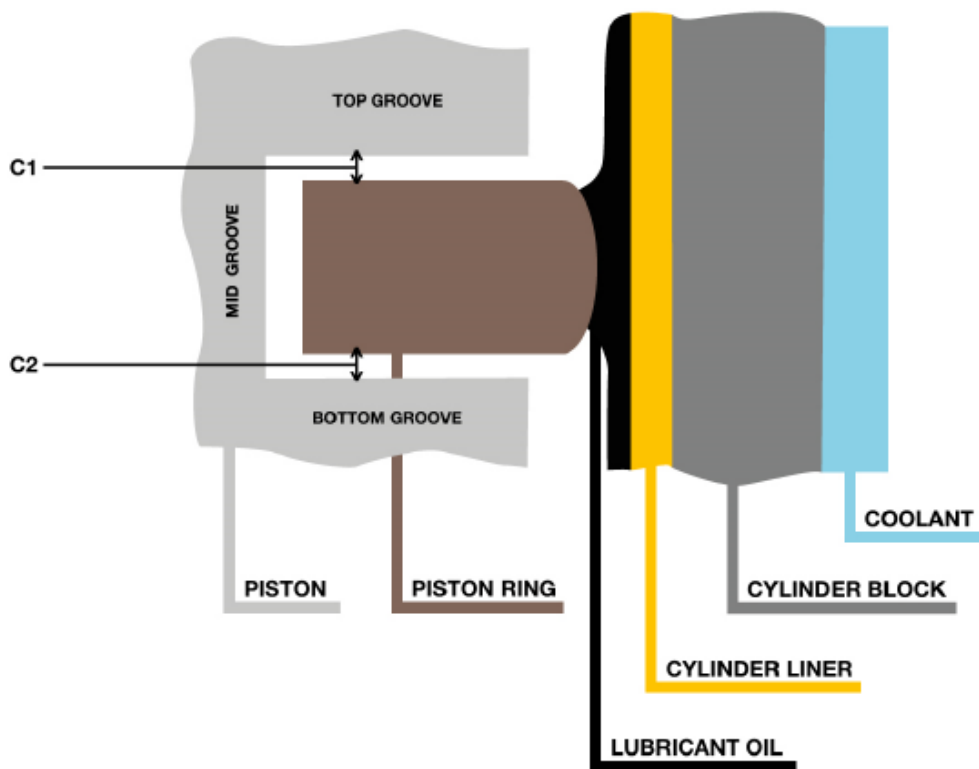


Figure 3.4 – Thermal circuit method [4]

3.1.4 Undercrown

Due to the complex geometry, different types of cooling, and the complexity of the fluid motion, it is hard to develop an empirical model able to describe the phenomenon in this region.

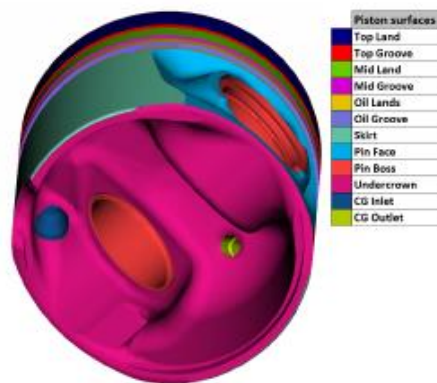


Figure 3.5 – Piston undercrown [4]

In [4] is showed the use of the Gnielinski's correlation with the assumption of turbulent flow in tubes based on eq 3.13:

$$Nu_D = \frac{\left(\frac{f}{8}\right)(Re - 1000)Pr}{1 + 12.7\left(\frac{f}{8}\right)^{\frac{1}{2}}(Pr^{\frac{2}{3}} - 1)} \quad (3.13)$$

Where Nu is the Nusselt number, Re is the Reynold number and Pr the Prandtl one, f is the Darcy factor, and it is expressed by the eq 3.14:

$$f = (0.79 \ln(Re) - 1.64)^{-2} \quad (3.14)$$

Finally, the HTC is expressed by taking into account the thermal conductivity k as shown below in eq 3.15:

$$h = kNu_d \quad (3.15)$$

3.2 INVERSE HEAT CONDUCTION METHOD

The inverse heat conduction method is an approach that, following an iterative procedure, permits to determine boundary conditions. It is used and presented in [4], [16], and [17] to determine thermal boundary conditions in steady-state thermal analysis, and in particular, to determine the heat transfer coefficients. It can be resumed in these following steps:

1. Start from an initial set of HTCs.
2. Perform a FEM simulation with these HTCs.
3. Calculate the thermal map and compare it with experimental measurements.
4. If the difference is too high, the HTCs are adjusted, and the simulation redone.
5. When the difference between calculated and experimental temperatures is acceptable, the iteration procedure ends.

This type of approach is very useful in all tuning procedure in which the calibration and the validation of the model is based on a comparison with experimental measurements. Here below in figure 3.6 is presented the flowchart.

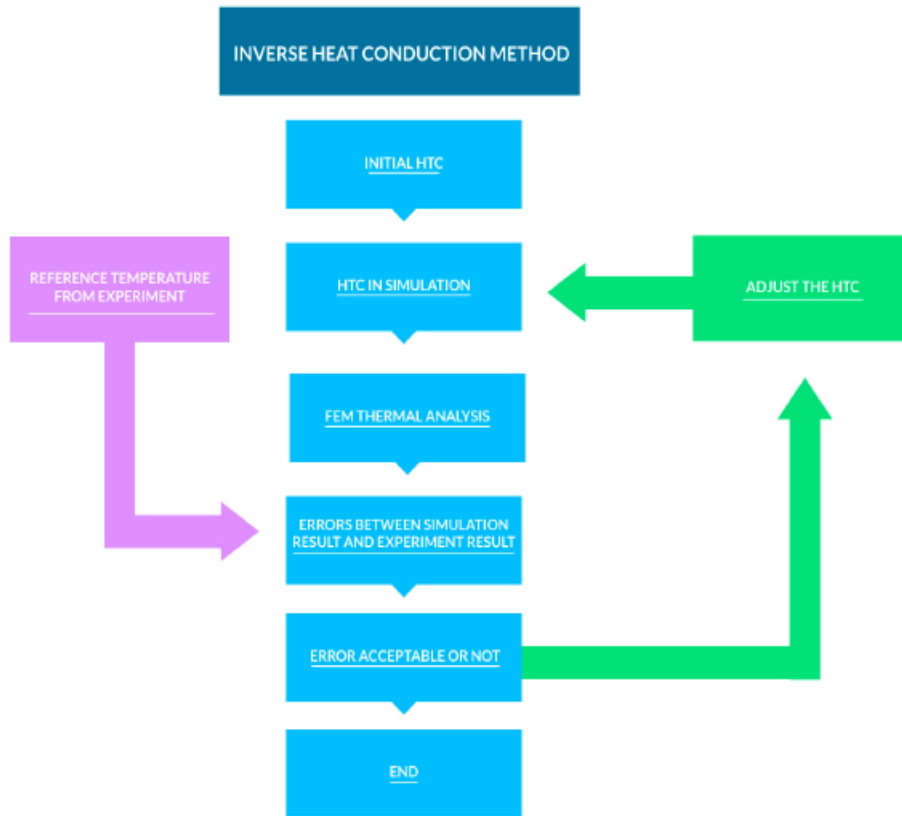


Figure 3.6 – IHCM flowchart [4]

The IHCM alone is not able to produce reliable results; it is needed a method to determine a correct starting HTC's family to have a fast convergency of results, and for this purpose can be used all the empirical correlations analyzed in previous chapters. The second important point is to establish a method to change the HTC's as a function of the resulted difference. To do it, it is possible to use mathematical algorithms for optimization. This was done by M. Gonera and O. Sadin in [4]; they have examined two algorithms, applying them on the IHCM, to determine HTC's. In particular, the two algorithms were:

1. Nelder-Mead simplex algorithm.
2. Levenberg-Marquardt algorithm.

The conclusion was that also if the second one is more powerful, it is not able to work with non-continuous variables such as HTC's, so the first one gives better results.

3.3 MEASUREMENTS TECHNIQUE

Another part of the literature investigation was to investigate measurement techniques that are currently used in the company. The research was focused on acquiring a greater knowledge about measurement instrumentation and the understanding of the provenience of the data needed for the tuning process. In particular, in the company are used mainly two methods:

- ❖ Templug.
- ❖ Telemetry.

3.3.1 Templug

The Templug is composed of a steel screw that is temperature-sensitive. It can provide the maximum temperature in the installed location. It is usually used in situations in which it is difficult to place correctly other types of instruments, such as the thermocouples. In [18], Daniel P. et al. showed that Templugs have an ideal cycle which has to be followed to obtain a higher accuracy, and there are two potential sources of errors:

1. Lack of accuracy in the time measurements.
2. Large temperature spikes.

For what concerns the first point, in [18] it is shown that Templugs are not so sensitive to time, and for a duration of the test greater than one hour, the maximum difference on the temperature is 2°C. For the second point, instead, the situation is the opposite; Templugs are very sensitive to temperature spikes even if they are very short.

3.3.2 Telemetry

Nowadays, there are a lot of different types of Telemetry systems. However, the base construction is based on a thermocouples system, and on a system that can in real-time, monitor and process all the signal values arriving from the thermocouple; the output is not a single value for every location but is a continuous function in the time of the acquired measure. They are less sensitive to temperature spikes but are difficult to place in some situations and have a higher cost.

3.3.3 Templug vs Telemetry

From the comparison of the two technologies in [18] is highlighted that the Templug claims an accuracy of 6% while the Telemetry claims a system accuracy of 4%. In the experiment carried out by Daniel P. et al. a piston is equipped with Telemetry's thermocouples and with sixteen Templugs, two for every location, an inner and an outer one; five of these Templugs resulted in a higher temperature evaluation with respect Telemetry, and all these fives were in the bowl region. This could be triggered by the steep thermal gradient that is present in that region, highlighting the fact that the Templugs application is less suitable with respect Telemetry for these regions or when it is present thermal gradient across the Templug. One way to reduce this error is to place the Templug closer to the position of the expected maximum temperature. In [19], Telemetry measurements are used to verify a piston model under full load condition; in this case, the difference between measured and calculated temperature was less than 5%, and the more significant difference was present in the piston top region so following what is discussed above.

3.4 LIMIT TEMPERATURE FOR Al ALLOYS

This section of the literature investigation was performed to better understand from where the internal company limit for Al-alloys sets to 400° C derives. Quite similar limit value is mentioned for Al-alloys pistons also in [20] and in [21] and corresponds to the 66% of the melting temperature of a generic Al-alloy that is

around 610 °C; exceeding this limit means have possible cracking or damage. Another explanation to this value is found in [2] regarding the fatigue resistance of the material, which drops by 80 %, as shown in figure 3.7; also, this consideration is aligned with internal company knowhow.

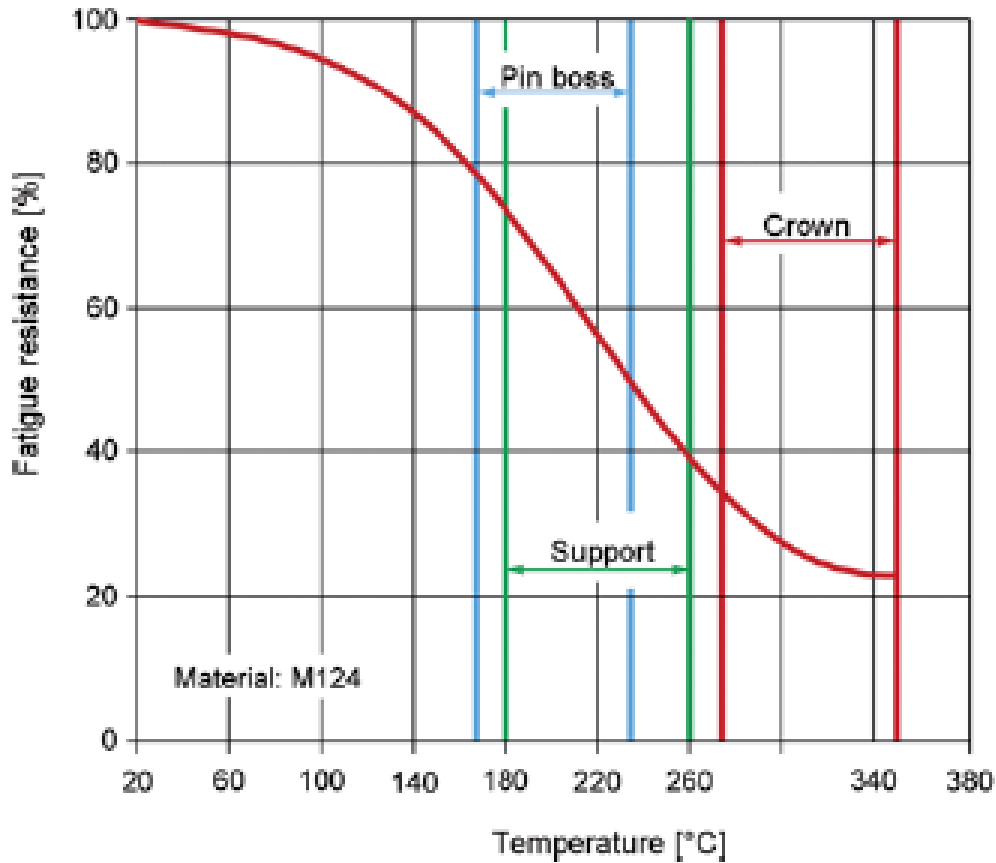


Figure 3.7 – Fatigue resistance of Al-alloys [2]

4 ACTUAL PROCEDURE ANALYSIS

The actual procedure investigation was done to understand the actual procedure itself better and also to determine which are the strong and the weak points. The whole analyzed process aims to obtain the so-called thermal map of the piston, to obtain a temperature value for each node of the mesh. These temperatures are after used for the thermal expansion and the complete thermo-mechanical fatigue analysis of the piston. The workflow of the actual procedure is shown in figure 4.1.

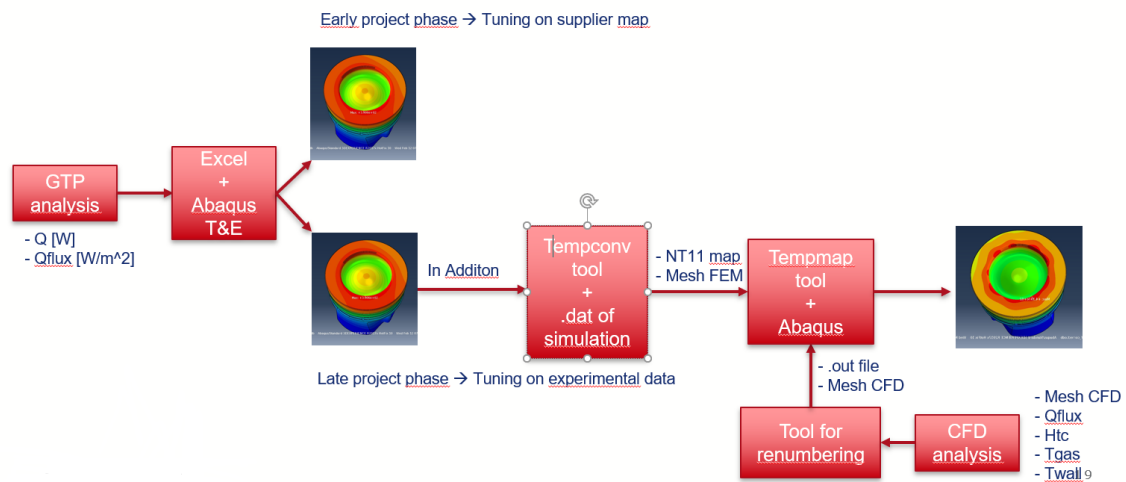


Figure 4.1 – Actual procedure workflow

Note: T & E → Trial and Error

4.1 GT-POWER TUNING

The procedure starts considering the boundary conditions from the GT-Power team that are obtained with the procedure showed in chapter 2.3.3 in a given point of the engine map; in particular, the examined condition is the peak power because it is the worst case.

Usually, these data are:

- ❖ Q [W].
- ❖ Qflux [W/m²].
- ❖ HTC [W/m² K].

- ❖ T_{gas} [K].
- ❖ T_{wall} [K].
- ❖ Area [mm²].

From the internal know-how of the company, the more reliable data are the Q and the Qflux, so the calibration procedure considers only these two boundary conditions from the GT-Power analysis. Since the GT-Power model is simplified (figure 4.2), the first step of the method is aimed to redistribute the Qflux according to the FEM model. This is done as follows:

1. Split the Qfluxes respecting the FEM model subdivisions.
2. Run the Abaqus simulations.
3. Check if Abaqus SOH=Q of GT-power.
4. If it is verified, the procedure is stopped.
5. If not, the Qfluxes are scaled in a linear way considering a scaling coefficient expressed by the ratio of the GTP Q and the Abaqus SOH, and the simulation is redone.

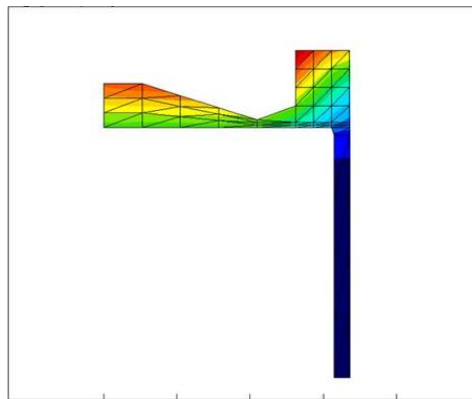


Figure 4.2 – GT-Power piston model

This is a trial and error procedure, done using Excel sheet and Abaqus simulations. Usually are required few iteration loops to obtain the correct results. At this point, to get the maximum temperature in the exact location, that is the bowl edge, and to have the cooling gallery working properly is done a further redistribution of the obtained Qfluxes with the same procedure explained previously; also, in this case, a small number of loops are required. The next step

of the procedure is the temperatures tuning of the model, and it is done to available data that usually are:

- ❖ Early project phase → Supplier map.
- ❖ Late project phase → Experimental data from Templugs or Telemetry.

This procedure is also a trial and error one, and it is done with the help of an Excel sheet and Abaqus simulations. The steps are the following:

1. Start with a HTC's family from a previous project.
2. Run the Abaqus simulation.
3. Check the difference between calculated and reference temperatures.
4. If it is less than 10° in all considered points, the procedure is stopped.
5. If not, the HTC's are changed basing on analyst experience and the simulation redone.

After a variable number of loops, the results is the one showed in figure 4.3.

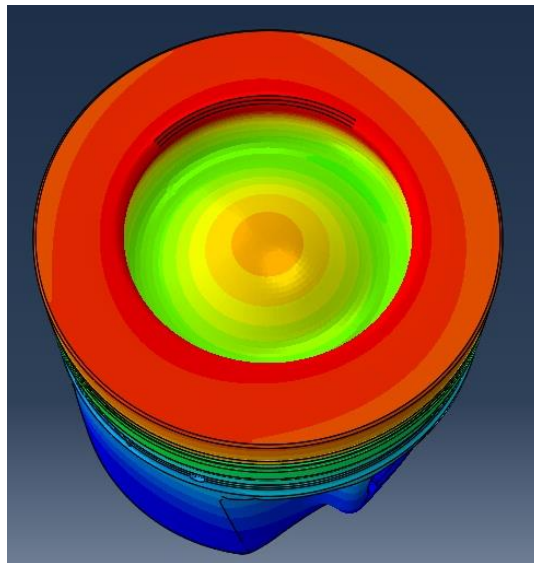


Figure 4.3 – GT-Power tuning thermal map

At this point, it is possible to highlight the strong and week point of the procedure:

- ✓ Good matching with experimental data.
- X Extremely variable number of loops.
- X Absence of injection points.

To obtain a correct temperature distribution and visible injection points, it has been developed a procedure that takes into account boundary conditions from CFD3D analysis. This procedure will be analyzed in the following chapter.

4.2 CFD3D TUNING

The first step of this second part of the procedure is to consider CFD3D boundary conditions provided by the CFD3D team, to solve the issue related to the distribution and the injection points. In this case, the analysis is performed, as explained in chapter 2.3.4. Usually, output data are:

- ❖ Nodes IDs and coordinates [mm].
- ❖ Qflux [W/mm^2].
- ❖ HTC [$W/mm^2 K$].
- ❖ Tgas [K]
- ❖ Twall [K].

The main difference is that in this case all these values are given for each node or element, and not for a region as for GT-Power, so the spatial distribution showed in figures 4.4 for HTCs, 4.5 for Tgas and 4.6 for Qflux is closer to the reality and more accurate.

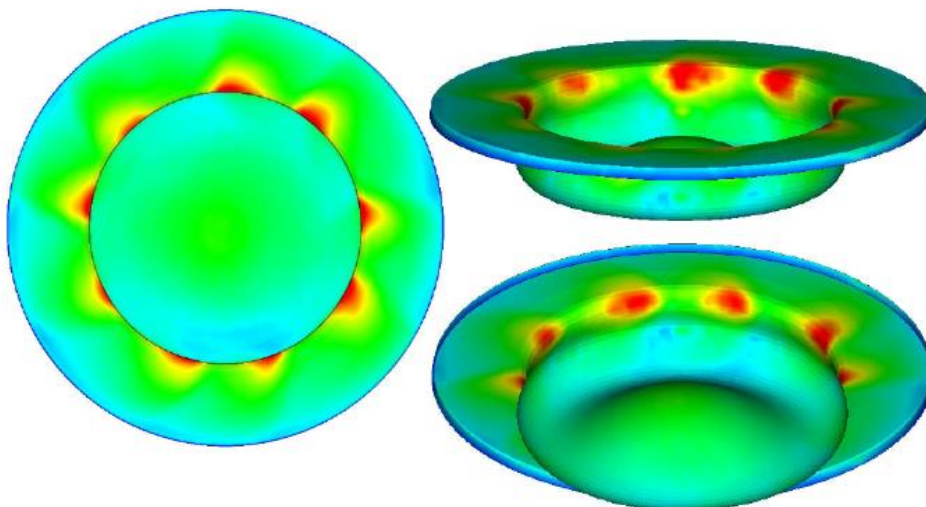


Figure 4.4 – CFD3D HTCs distribution

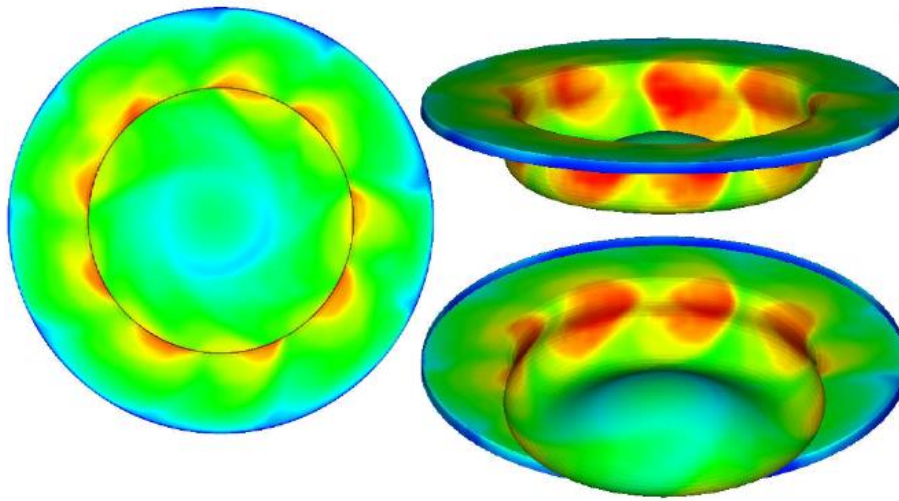


Figure 4.5 – CFD3D Tgas distribution

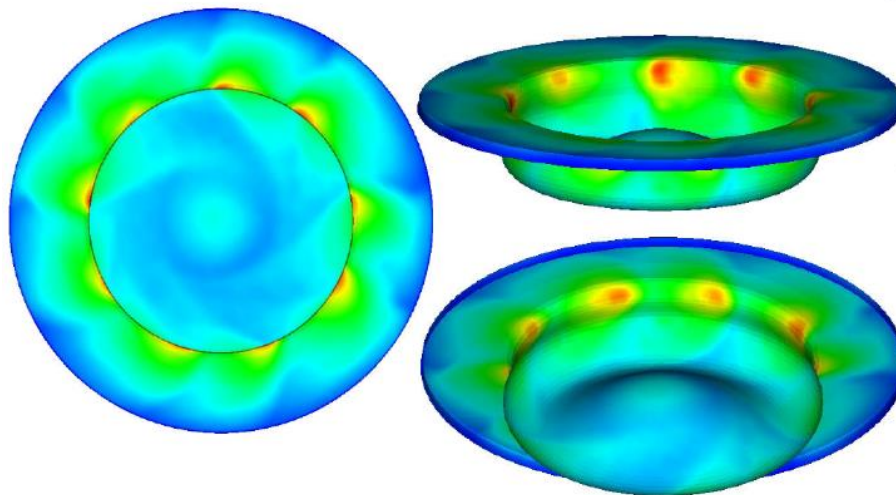


Figure 4.6 – CFD3D Qflux distribution

In this way are obtained visible injection points, but to use this data, some issues are to be solved:

- ❖ Use a previous thermal map for wall temperatures to have a fast convergency of the results.
- ❖ Match the CFD3D and the FEM different meshes.

In the actual procedure, the first issue is solved, taking the .dat file of the previous simulation tuned on GT-Power, and with the help of an internal tool, wall temperatures are obtained. For what concerns the second point, instead, it is

taken the .out file in which there are all the quantities coming from the CFD3D analysis, and with an in-house developed MatLab code, it is adjusted the numeration of the nodes of the mesh to have the correct matching. The final step is to use another internal tool that receives in input four files:

- ❖ FEM mesh.
- ❖ CFD3D mesh.
- ❖ .out file of CFD3D BCs.
- ❖ Wall temperatures.

This tool creates an Abaqus card with a Qflux for each element, starting from nodal quantity used in the Abaqus steady-state thermal analysis. The result is showed in figure 4.7.

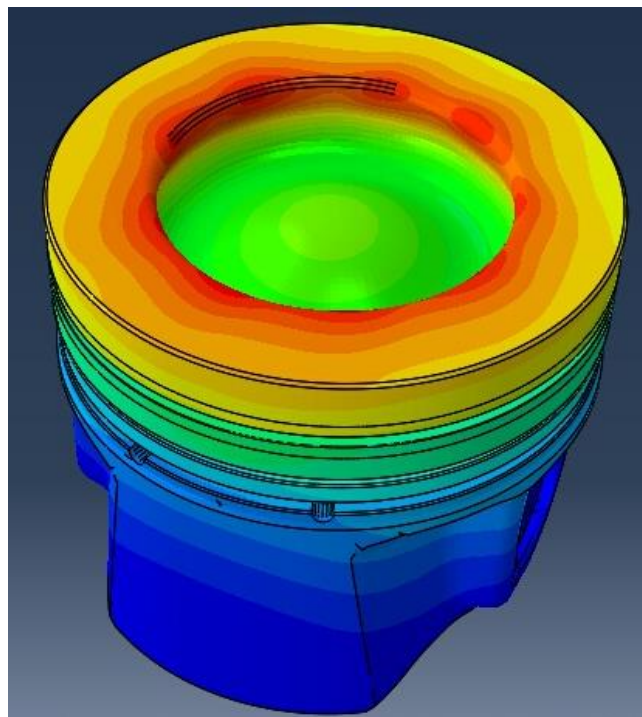


Figure 4.7 – CFD3D tuning thermal map

As it is done before it is possible to highlight the strong and the week point of this procedure:

- ✓ Visible injection points
- X Temperatures are much higher with respect to GT-Power tuned ones.

- X The procedure needs many tools.
- X The procedure always needs the previous tuning based on GT-Power.
- X Variable loop number.

5 CROSS-FUNCTIONALITY MEETING

This chapter describes the cross-functionality meetings that were done to understand better where BCs came from and the reliability of the BCs themselves. Many meetings were done with GT-Power and CFD teams, and the procedure used to obtain the BCs is the other outcome of this step, and it is described in chapters 2.3.3. and 2.3.4.

5.1 CROSS-FUNCTIONALITY MEETING: GT-POWER

For what concerns the GT-Power BCs are composed by:

- ❖ Q [W].
- ❖ Qflux [W/m²].
- ❖ HTC [W/m² K].
- ❖ Tgas [K].
- ❖ Twall [K].
- ❖ Area [mm²].

In particular, in the actual procedure, the BCs that are used are the Q and the Qflux, so at this point, the questions were: Are these two the most reliable data that can be used? Which of the two is the better one? Are there also other BCs that can be used? Analyzing the procedure deeply are highlighted the following considerations:

- ❖ Being a 2D symmetrical model, the Area parameter is not accurate, and especially when there are stepped bowls or complex geometries, the difference with respect to the FEM and the real one is too much.
- ❖ As a consequence of the previous points, the Qflux is not so reliable because the area parameter influences it.
- ❖ For what concerns the HTCs and the Tgas, both are calculated with a cycle average 0D model but are computed on a region and not in a punctual way, so basically are less accurate with respect CFD3D ones.

- ❖ T_{wall} is imposed based on a previous project and on internal experience, also for T_{gas} and for the HTC_s is imposed on a whole region.
- ❖ Q is obtained with a thermodynamic balance that takes into account the whole engine and so all the heat transfer processes. It is also from the internal know-how of the company that results quite reliable.

In the end, it can be said that the most reliable BC coming from the GT-Power team is the Q, also in this case; however, it is calculated the total, and it is split into different regions, so it is more accurate to refer to the Q_{tot}. The T_{wall} can also be taken into considerations in situations in which there are no other indications.

5.2 CROSS-FUNCTIONALITY MEETING: CFD3D

CFD3D BCs are composed by:

- ❖ Nodes IDs and coordinates [mm].
- ❖ Q_{flux} [W/mm²].
- ❖ HTC [W/mm² K].
- ❖ T_{gas} [K]
- ❖ T_{wall} [K].

In this case, all these BCs are used in the actual procedure except for the T_{wall}, for which it is used one thermal map coming from the GT-Power and FEM analysis. In this case, all the BCs are obtained punctually, and being a 3D model is more accurate and can correctly reproduce the real geometry of the combustion chamber. The questions were the same as the previous chapter, but also it has been investigated and the interaction between two different meshes coming from two different software. The conclusions are the following:

- ❖ The situation is the opposite with respect to the previous one, so the most reliable parameters are the Q_{flux} that comes from a fluid-dynamics analysis, the HTC_s, and also the geometry parameter.

- ❖ The T_{gas} parameter is the one that can be more affected by errors because it is influenced by many factors, as explained in chapter 2.3.4.
- ❖ The T_{wall} parameter can be taken from GT-Power and so regional, and in this case, the reasoning is the one done before, or it can be taken from the previous loop, and in this case, it can be more accurate because it is punctual.
- ❖ For what concerns meshes interaction, the problem is influenced by how are given the BCs. This topic will be analyzed and discussed deeply later.

In the end, all these BCs can be used, paying particular attention to the choice of the T_{wall} and on the choice of the type in which BCs are given.

5.3 CFD3D & GT-POWER INTERACTION

It is evident that there is a strong interaction between GT-Power and CFD3D analyses, indeed as explained in chapter 2.3.4, the CFD analysis is calibrated on the p , T , and HRR traces coming from the GT-Power model. Moreover, there is also the issue related to the T_{wall} . When the CFD team does not have any T_{wall} coming from one previous project, they imposed that one equal to the GT-Power one. In the actual procedure, it is considered a scaling factor applied in Abaqus that multiplies all the heat fluxes; this scaling factor is obtained as the total GT-Power heat is uniformly distributed on the piston crown. Another interaction is the use of a thermal map coming from one previous GT-Power/Abaqus analysis to be used in the actual procedure as T_{wall} , in [4] it is imposed that temperature and heat transfer coefficient distributions are modified to match the GT-Power one. All these considerations lead to define that this interaction is of fundamental importance, and that can be improved and optimized. In the end, the most promising way is to consider the GT-Power Heat (Q), and the other parameters are taken from the CFD3D analysis.

6 NEW PROCEDURE PROPOSAL

After having analyzed the actual procedure and after having done all the cross-functionality meetings, a new method has been proposed. This new procedure tries to solve and to optimize all the issues related to the actual one, with considerations based on what highlighted in previous chapters. In particular, the new procedure has a new optimized workflow and a new tool that contains all the functions done by many different tools in the actual procedure. The main goals of these steps were:

- ❖ To use in a more correct way the BCs coming from the CFD3D analysis to obtain a more realistic thermal map.
- ❖ To also consider the BCs coming from the GT-Power model to solve the issue of the temperatures overestimation.
- ❖ To solve the issue of the two different meshes.
- ❖ To optimize and speed up the whole process.

6.1 NEW WORKFLOW

The new proposed workflow tries to reduce the minimum number of tuning procedures without losing results accuracy. As said in chapter 5.1 the most reliable BC coming from GT-Power is the Q [W], so the whole trial and error procedure based on the Q flux was cut because using CFD3D BCs it is directly punctually obtained a correct heat distribution; moreover using the CFD3D BCs and so a 3D model it is possible to model the real geometry of the piston and so to have visible injection points. The interaction with GT-Power is still present because as said before the CFD3D analyses are calibrated also taking into account GT-Power traces of p , T , and HRR ; also since the GT-Power Q from the internal company know-how is more accurate in the new procedure all the BCs coming from the CFD3D analysis are scaled to match the GT-Power Q as follows:

1. At each wall surface node j , the following data is available for each time step (crank angle) i

$$q_{ij} [W/m^2], \quad h_{ij} [W/m^2K], \quad T_{gas\ ij} [K], \quad T_{wall\ ij} [K]$$

2. After averaging over the engine cycle, the following data is available at each wall surface node j

$$q_j = \frac{\sum_{i=1}^n q_{ij}}{n} \quad h_j = \frac{\sum_{i=1}^n h_{ij}}{n} \quad T_{gas\ j} = \frac{\sum_{i=1}^n T_{gas\ ij} h_{ij}}{\sum_{i=1}^n h_{ij}} \quad T_{wall\ j} = \frac{\sum_{i=1}^n T_{wall\ ij}}{n}$$

3. With these definitions, it follows that

$$q_j = h_j(T_{gas\ j} - T_{wall\ j})$$

$$Q_{TOT} = \sum_{j=1}^m q_j A_j$$

4. A method to scale Qtot to Qtot'=cQtot, through a scaling factor c, is to scale q at each node, scaling Tgas

$$q'_j = cq_j = h_j(c_{1j}T_{gas\ j} - T_{wall\ j}) = h_j(T'_{gas\ j} - T_{wall\ j})$$

$$c_{1j} = \frac{[c(T_{gas\ j} - T_{wall\ j}) + T_{wall\ j}]}{T_{gas\ j}}$$

5. Differences at each node j are the following

$$T_{gas\ j} - T'_{gas\ j} = (1 - c)(T_{gas\ j} - T_{wall\ j})$$

$$q_j - q'_j = (1 - c)q_j$$

The method:

- ❖ Does not change the distribution of q qualitatively, so high flux regions remain with high flux.
- ❖ Change the values and gradients of Tgas and q.
- ❖ Does not change the values and the spatial distribution of h.

The other main goal was to solve the problem related to the different meshes, in fact, in the actual procedure, there are the FEM structural mesh and the CFD3D one, and they have:

- ❖ Different number of elements and nodes.
- ❖ Different reference systems.
- ❖ Different numeration.

All these issues are solved using different tools that can match these meshes. In particular, it has to be said that the BCs given by the CFD3D team in the actual procedure are nodal quantities and so it is needed a tool that converts it into elements quantities because the Abaqus card needs quantities given in this way. In the new procedure, all these issues are solved differently:

- ❖ Instead of using two different meshes is used the same one, so the FEM one is given to the CFD3D team that with the use of Converge can remap BCs coming from the CFD3D analysis on that one. In this way, the nodes and the number of elements remain the same.
- ❖ All the quantities are given element by element, so there is no need to calculate them starting from nodal one, and the results are more accurate.
- ❖ The problem related to the different reference systems and the renumbering are solved using one unique tool that can roto-translate the mesh and to renumber nodes and elements.

This new tool will be analyzed in the following chapter. Using this new tool and Abaqus is obtained a new thermal map that still needs calibration, but the number of the tuning procedures is reduced. In figure 6.1 is showed the workflow of the new procedure.

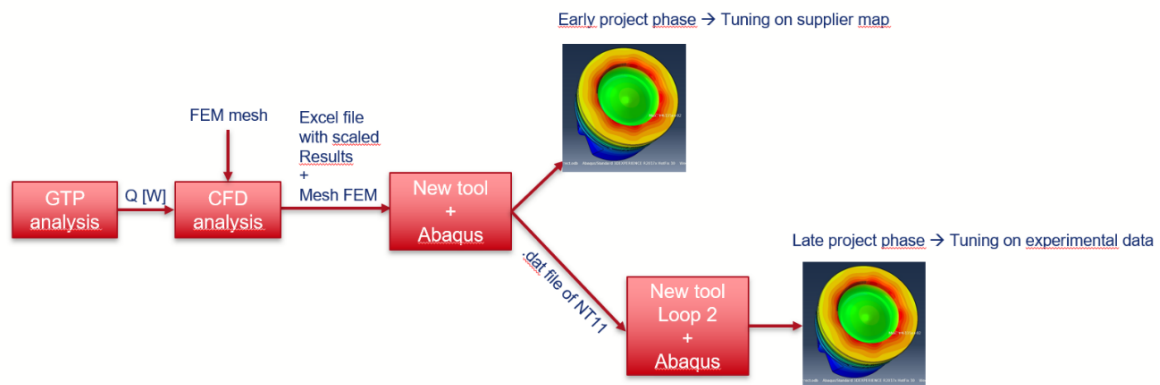


Figure 6.1 – New procedure workflow

6.2 NEW TOOL AND CORRESPONDENT FLOWCHART

The development of a new tool supports the new procedure. This new tool was developed to include all the steps done by many tools in the actual procedure, taking into account the diversity of the data used in the two procedures. The tool was developed in MatLab, while the ones of the actual procedure were developed in Fortran. It was also created a flowchart of the tool shown in figure 6.2, and in this way, it can be easily reprogrammed in all other programming languages. In particular, the tool receives as input the file of the FEM mesh, and a file with the BCs coming from the CFD3D analysis and perform the following steps:

1. Roto-translate the mesh to have the same reference system.
2. Renumber the BCs file to have matching with the FEM mesh.
3. Extract the T_{wall} from a .dat file coming from another simulation.
4. Calculate the Q_{fluxes} elements by elements.
5. Scale the Q_{fluxes} as showed before to match the GTP Q.
6. Generate the Abaqus card to perform the analysis.

The results coming from this new procedure and this new tool will be analyzed and presented in the following chapters with application on real cases.

SECTION 1 LOAD FEM DATA

SECTION 2 LOAD CFD DATA

SECTION 3 LOAD THERMODYNAMIC DATA

SECTION 4 ROTOTRANSFORMATION

SECTION 5 RENUMBERING & REMAPPING

SECTION 6 T_{wall} & Q_{flux} CALCULATION

SECTION 7 ABAQUS CARD

Figure 6.3 – New tool flowchart legend

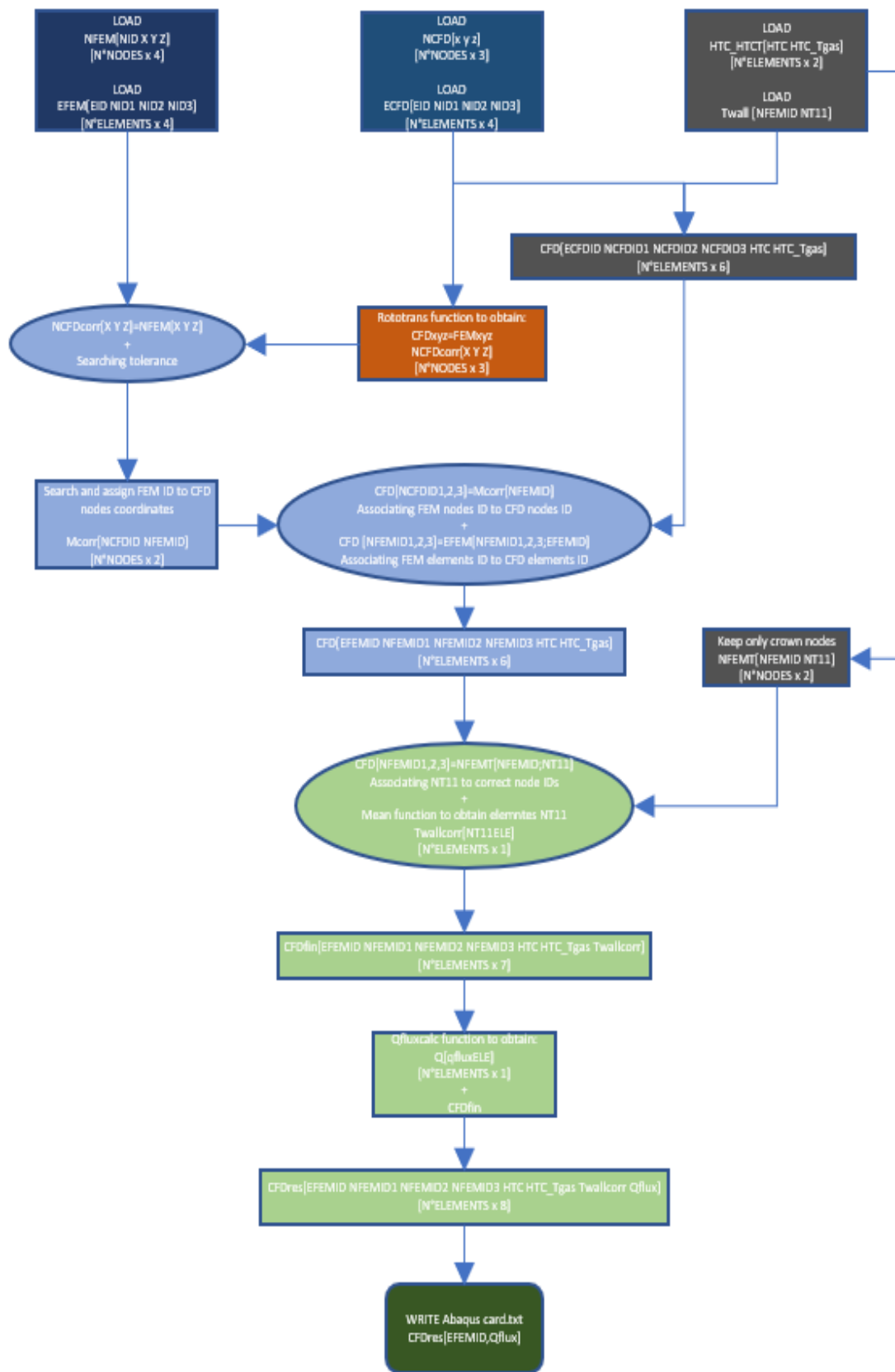


Figure 6.2 – New flowchart

Here below is figure 6.4 is showed an example of the thermal map obtained with the use of this new procedure and with the new tool.

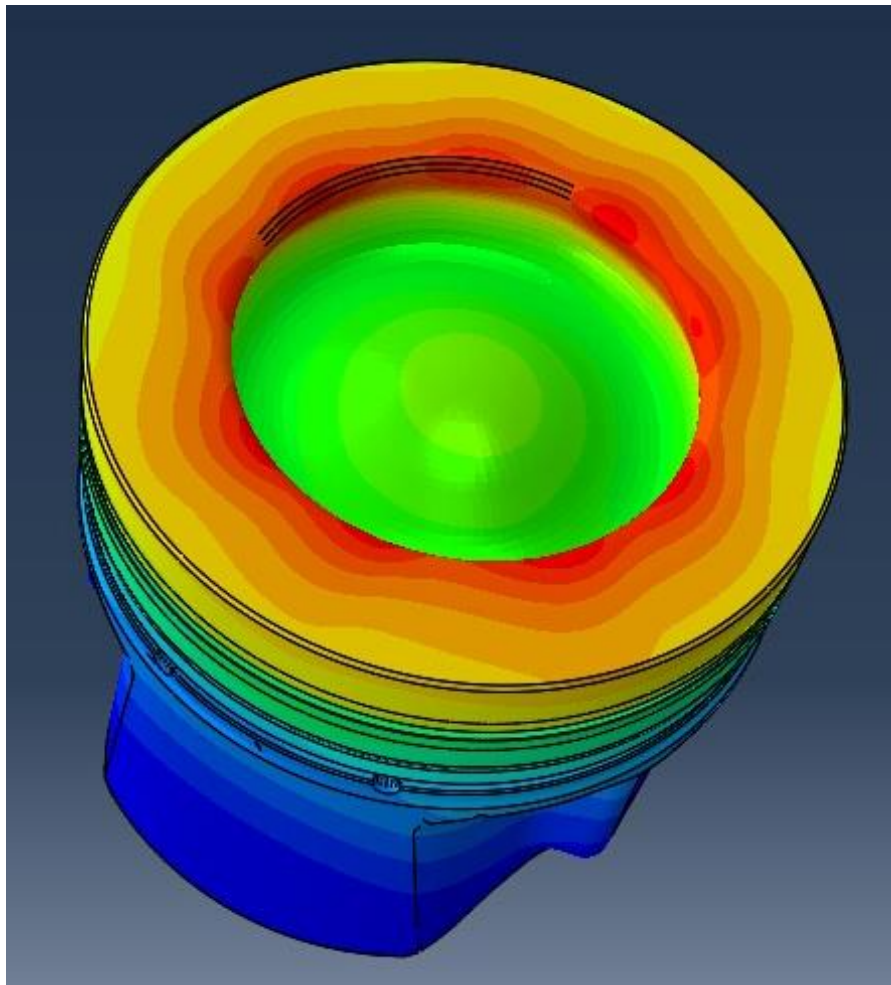


Figure 6.4 – Thermal map with new tool and procedure

6.3 PROCEDURE COMPARISON

This chapter analyzes the main differences between the actual procedure and the new one, in particular, the focus is on the workflow and all the steps of the procedure. The differences and the improvements related instead to the numerical results will be analyzed in the following chapter concerning two different case studies. In figures 6.5 and 6.6 below are highlighted strong and weak points of the two procedures.

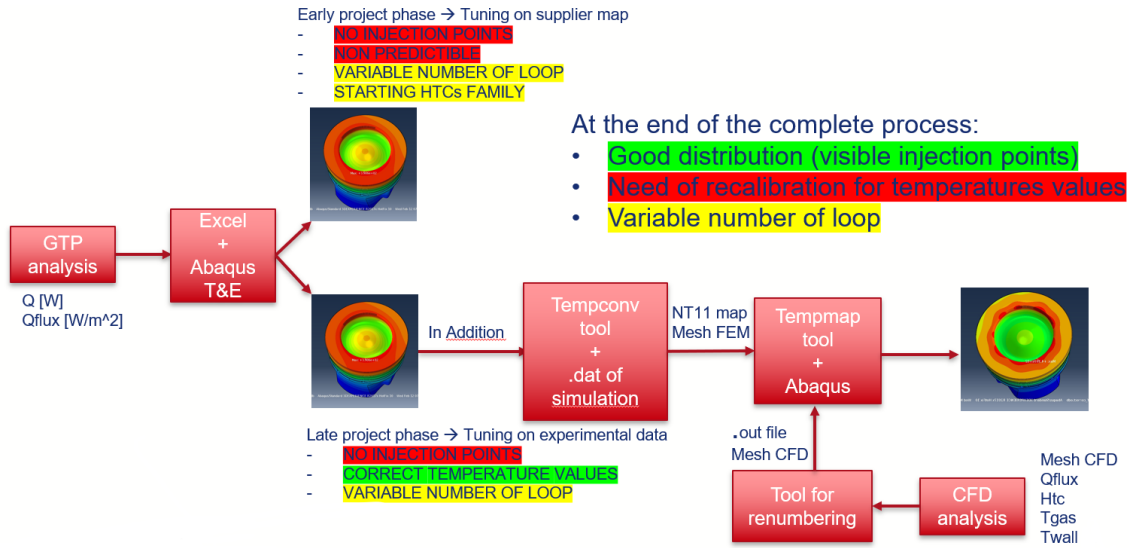


Figure 6.5 – Actual procedure

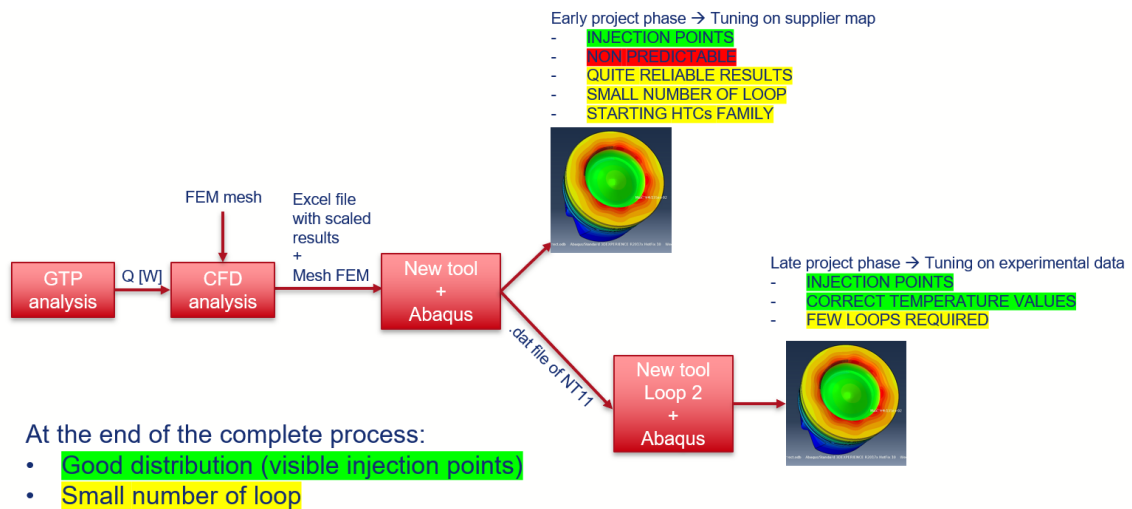


Figure 6.6 – New procedure

From the chart, it is possible to see how the new procedure is an improvement of the previous one. Indeed, the process is more linear, and the whole trial and error procedure is cut. Moreover, the direct interaction with the GT-Power analysis is substituted with the interaction only with the CFD3D team, but as said before, with the scaling coefficient described in chapter 6.1, the GTP model results are used.

The differences in the early project phase are:

- ❖ Presence of visible injection points.
- ❖ More reliable results.
- ❖ Smaller number of tuning loops.

The problem related to the model's predictivity and to the starting HTC's family are still present, and in the future work chapter, some solutions to these issues will be proposed. In the late project phase instead, the differences are:

- ❖ Presence of visible injection point if it is considered only the GTP tuning in the actual procedure.
- ❖ A smaller number of tuning loops.

In the end, the new procedure reduces the number of tuning procedure and iterative loops, it is more straightforward, and the data cleaning procedure has reduced a lot the number of files that have to be used and generated. Here below in table 6.1 are highlighted these considerations counting the steps of the two procedures; indeed, the tuning procedures are reduced by 66% while the steps are reduced by 44%. The yellow cell represents a tuning procedure that usually requires a small loop, while the orange ones require a variable number of loop.

OPERATIONS COUNT	STANDARD PROCEDURE	SUBROUTINES			OUTPUT FILE
1	Tuning on GTP Q	Abaqus analysis	Check SOH	Qflux Redistribution	
2	Tuning on experimental measurements	Abaqus analysis	Check NT11	HTC change	.dat
3	Tempconv				.aba temp
4	Rototranslation				
5	Export crown FEM mesh				.nas
6	Export crown CFD mesh				.nas
7	Renumbering CFD mesh				.out
8	Tempmap				.aba
9	Tuning on experimental	Abaqus analysis	Check NT11	HTC change	END

OPERATIONS COUNT	NEW PROPOSAL PROCEDURE	SUBROUTINES			OUTPUT FILE
1	Export crown FEM mesh				.inc
2	Crownmap				.aba
3	Abaqus	Abaqus analysis			.dat
4	Crownmap Loop2				.aba
5	Tuning on experimental	Abaqus analysis	Check NT11	HTC change	END

N° STANDARD PROCEDURE OPERATIONS	9
N° NEW PROCEDURE OPERATIONS	5
% OPERATIONS REDUCTION	-44

N° TUNING STANDARD PROCEDURE	3
N° TUNING NEW PROCEDURE	1
% TUNING REDUCTION	-67

Table 6.1 – Procedure comparison

7 INLINE 6 CYLINDER AL-ALLOY PISTON CASE STUDY

In this chapter is analyzed an Al-alloy piston for an inline six cylinders Diesel engine. The steps followed to obtain the results showed here are the ones described in previous chapters, so the discussion starts with the GT-Power tuning, and after with the CFD3D tuning following the actual procedure. In the end, are discussed the results obtained with the new procedure. Here below in figure 7.1 is showed the FEM mesh model of the piston, while in figure 7.2 are showed the Telemetry sensors position.

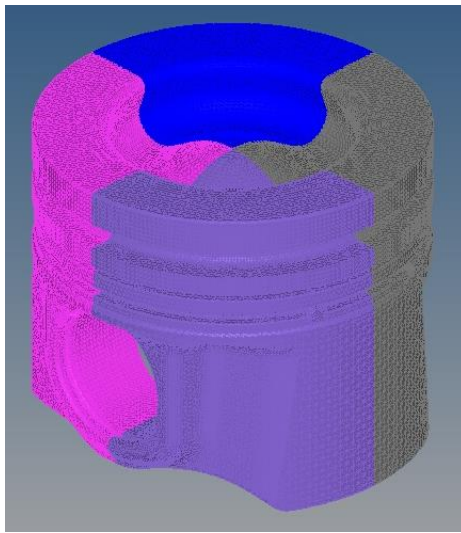


Figure 7.1 – Piston FEM mesh

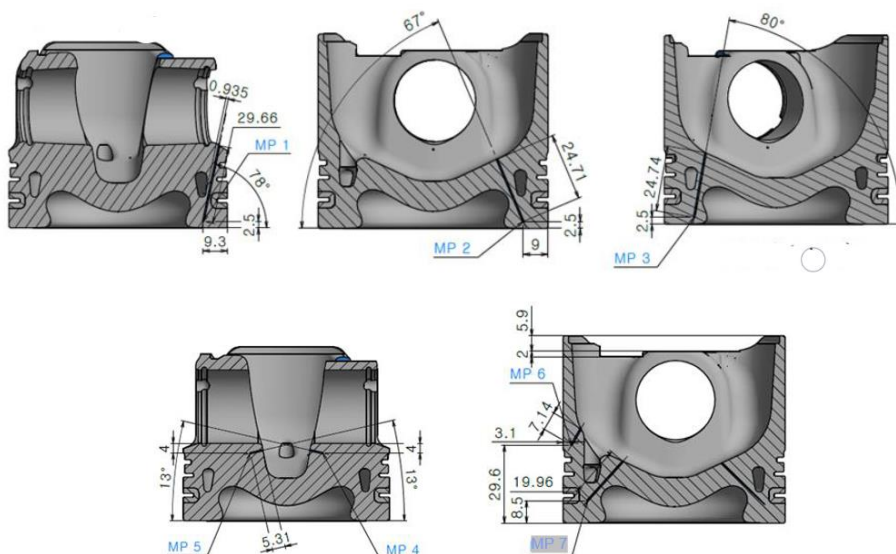


Figure 7.2 – Telemetry sensors

7.1 GT-POWER TUNING

The first step is the GT-Power tuning, and as explained before, in the first phase, the Qfluxes are redistributed, the simulation is performed, and the check is done between simulation SOH [W] and Gt-Power Q [Q]. The next step consists in to modify the different Qfluxes region by region to obtain the maximum temperature in the correct zone. After these steps, the situation is the one reported here below in table 7.1.

POSITION	Telemetry	GTP Tuning Loop 1	
		FEA Temperature	Difference vs. Telemetry
[-]	[°C]	[°C]	[°C]
MP1 Crown1 TS R	352	362	3
MP2 Crown1 ATS F	318	360	12
MP3 Crown ATS R	373	365	-2
MP4 Undercrown R	235	226	-4
MP5 Undercrown F	235	226	-4
MP6 Skirt	160	159	-1
MP7 ALFIN ATS	320	320	0
MAX		393	

Table 7.1 – 1st Loop GTP

It has to be said that the second sensor was a failed one, so it is highlighted in red and considered for the calibration procedure in all the cases. In this table, all the results have a temperature difference of less than 10°C and a maximum temperature of less than the limit of 400°C. At this point starts the real calibration procedure aimed to reduce these differences, so the HTCs are modified, and the simulation is redone. After several loops, the final calibration is the one showed in table 7.2.

POSITION	Telemetry	GTP Tuning Final Loop	
		FEA Temperature	Difference vs. Telemetry
[-]	[°C]	[°C]	[°C]
MP1 Crown1 TS R	352	351	0
MP2 Crown1 ATS F	318	345	8
MP3 Crown ATS R	373	365	-2
MP4 Undercrown R	235	232	-1
MP5 Undercrown F	235	231	-2
MP6 Skirt	160	160	0
MP7 ALFIN ATS	320	319	0
MAX		390	

Table 7.2 – Final Loop GTP

In this case, the temperature differences are all less than 8°C, and the maximum temperature at the bowl edge is equal to 390°C. In figures 7.3, 7.4, and 7.5 is shown the thermal map obtained from this procedure.

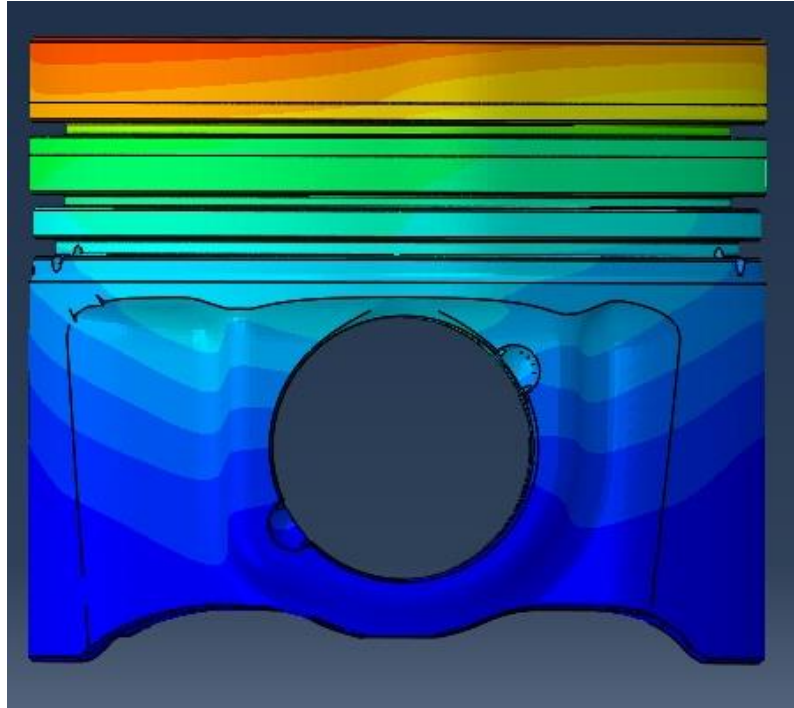


Figure 7.3 – Thermal map GTP front

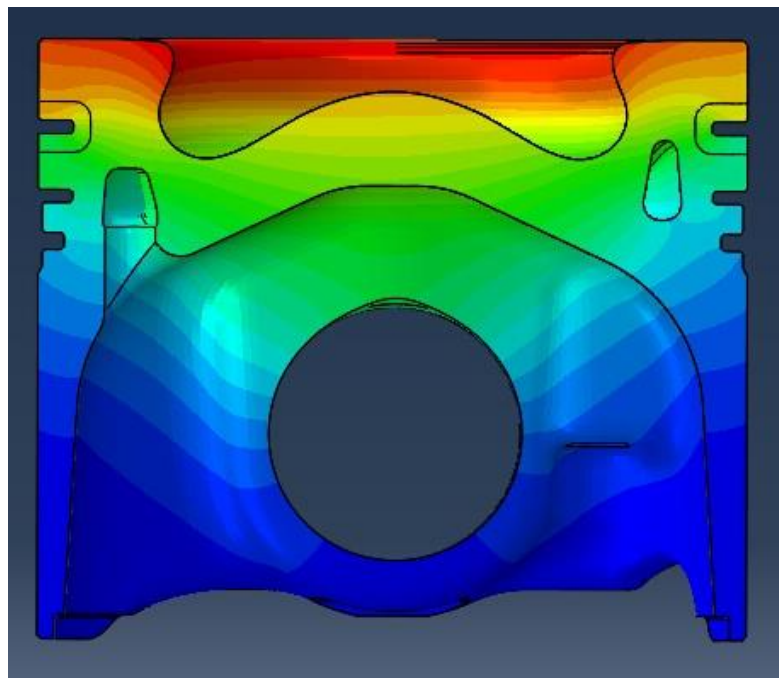


Figure 7.4 – Thermal map GTP front section

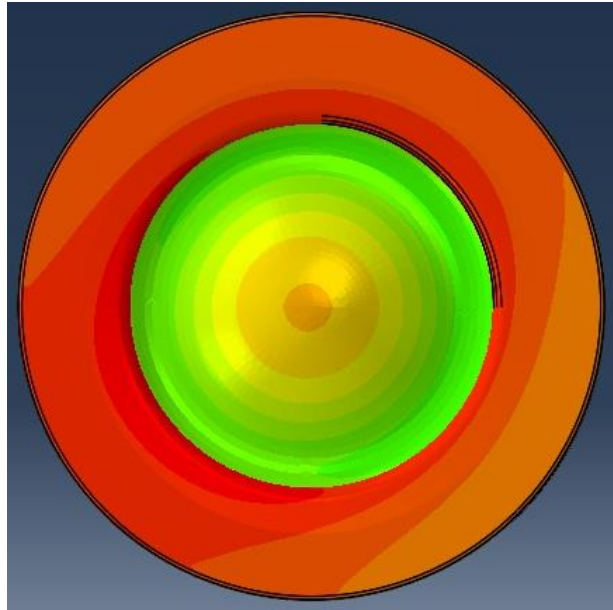


Figure 7.5 – Thermal map GTP crown

As shown in these figures, there are no visible injection points, so the temperature distribution is in accordance with experimental data numerically speaking, but the qualitative result is not realistic.

7.2 CFD3D TUNING: ACTUAL PROCEDURE

This part of the procedure is used to obtain a more realistic temperature distribution and visible injection points. Following the process described in chapter 4.2 and using all the tools that are needed, it is obtained an Abaqus card which contains the heat fluxes element by element, at this point the simulation is launched. The results are shown in table 7.3.

POSITION [-]	Telemetry [°C]	CFD Standard Tuning	
		FEA Temperature [°C]	Difference vs. Telemetry [°C]
MP1 Crown1 TS R	352	366	4
MP2 Crown1 ATS F	318	367	13
MP3 Crown ATS R	373	382	2
MP4 Undercrown R	235	225	-4
MP5 Undercrown F	235	227	-4
MP6 Skirt	160	161	1
MP7 ALFIN ATS	320	333	4
MAX		440	

Table 7.3 – CFD3D tuning

In this case, the differences are low, less than 15°C, but higher with respect to the GT-Power calibration. Another significant result is the maximum temperature that, in this case, is equal to 439.7°C and so over the internal company limit. Here below in figure 7.6, 7.7, and 7.8 is shown the temperature distribution. In this analysis, the T_{wall} are taken from the previous GTP calibration shown in table 7.2.

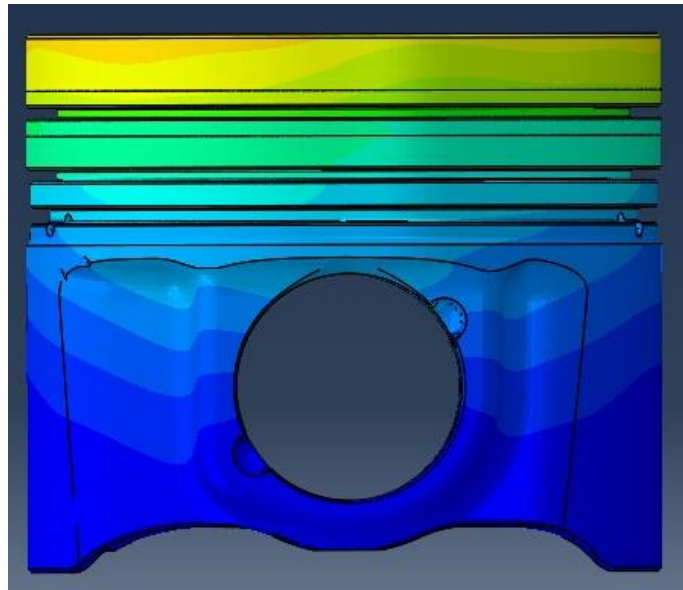


Figure 7.6 – Thermal map CFD3D front

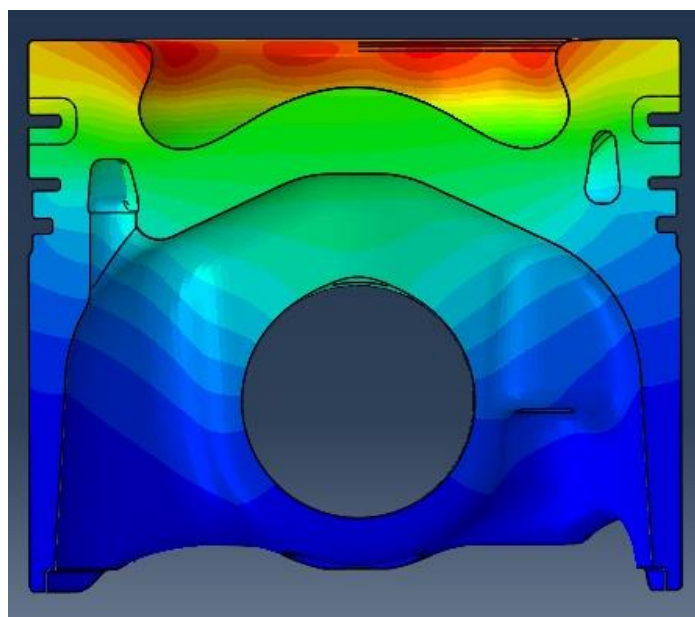


Figure 7.7 – Thermal map CFD3D front section

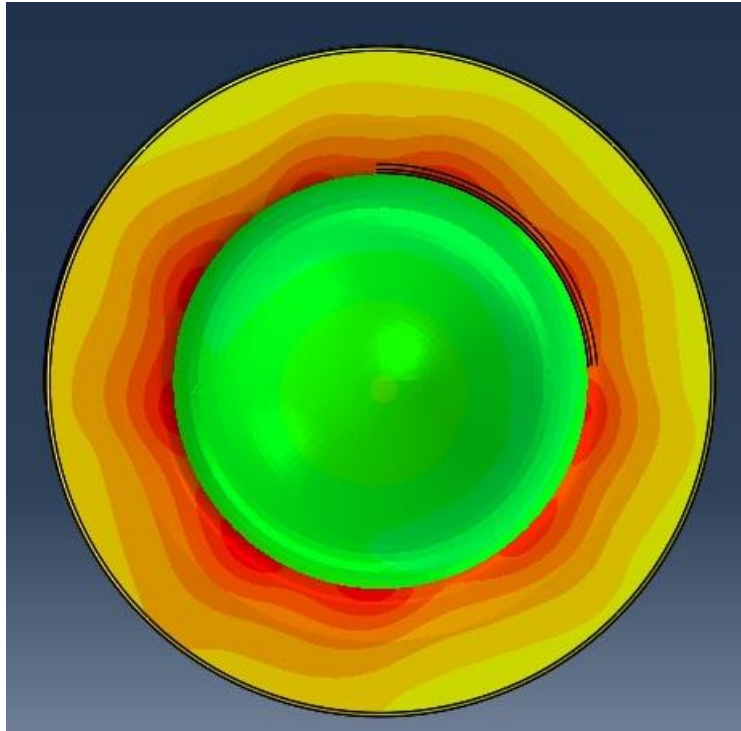


Figure 7.8 – Thermal map CFD3D crown

In this case, all the injection points are visible, and the thermal map is more realistic compared to the previous one. Moreover, to reduce the temperature differences and the maximum temperature, more tuning loops are needed, and in some cases the whole calibration procedure has to be repeated. In all these simulations, the starting HTC's family is the one derived from the GTP calibration procedure.

7.3 NEW TOOL TUNING

In this chapter, the case study is performed following the new proposal procedure, so following these considerations:

- ❖ The mesh is the same for the FEM and the CFD3D analysis.
- ❖ The CFD3D BCs are given element by element.
- ❖ The BCs are scaled taking into account the GTP $Q[W]$
- ❖ The new tool is used.
- ❖ Three different T_{wall} are used:

1. GTP thermal map from the previous simulation. (Table 7.2)
2. Constant T_{wall} equal to the CFD3D constant one.
3. Thermal map coming from the first loop with case 2) T_{wall}.
(iterative procedure)

The results coming from the case 1) are reported in table 7.4 here below. In this case, the differences are higher with respect to other cases, especially in the undercrown region where the temperature difference is around 20°C, and also in the anti-thrust side rear part of the crown in which the difference is 21°C. In all the other regions, differences are less than 7°C, and the maximum temperature is equal to 413.5°C.

POSITION [-]	Telemetry [°C]	CFD New Tool GTP thermal map	
		FEA Temperature [°C]	Difference vs. Telemetry [°C]
MP1 Crown1 TS R	352	345	-2
MP2 Crown1 ATS F	318	348	9
MP3 Crown ATS R	373	352	-6
MP4 Undercrown R	235	216	-9
MP5 Undercrown F	235	217	-8
MP6 Skirt	160	156	-2
MP7 ALFIN ATS	320	312	-2
MAX		414	

Table 7.4 – CFD3D new tool tuning GTP thermal map

In case 2) the situation is different, indeed, the temperature differences are lower in the undercrown region, and also in the anti-thrust side rear region of the crown. In the other zones, the differences are slightly higher and around 13°C for two sensors, and less than 4°C for the other two. The maximum temperature in this case is equal to 443 °C. The results are shown in table 7.5.

POSITION [-]	Telemetry [°C]	CFD New Tool Constant T _{wall}	
		FEA Temperature [°C]	Difference vs. Telemetry [°C]
MP1 Crown1 TS R	352	365	4
MP2 Crown1 ATS F	318	366	13
MP3 Crown ATS R	373	376	1
MP4 Undercrown R	235	222	-6
MP5 Undercrown F	235	218	-8
MP6 Skirt	160	160	0
MP7 ALFIN ATS	320	331	3
MAX		443	

Table 7.5 – CFD3D new tool tuning constant T_{wall}

In the last case, the T_{wall} temperatures are obtained following the late project phase of the new proposal procedure, so the thermal map used is the one obtained from the first loop that, in this case, is represented by the case 2). The results are shown in table 7.6. It can be seen that the regions in which the temperature differences are high are the same as in the previous cases, and the different values are close to the ones of the case 1). In all other regions, the temperature differences are less than 4°C, and the maximum temperature is equal to 416.5°C. This demonstrates that the first tuning part of the actual procedure, used in case 1), can be avoided, with a significant time saving, obtaining comparable results.

POSITION [-]	Telemetry [°C]	CFD New Tool Loop 2	
		FEA Temperature [°C]	Difference vs. Telemetry [°C]
MP1 Crown1 TS R	352	348	-1
MP2 Crown1 ATS F	318	349	9
MP3 Crown ATS R	373	357	-5
MP4 Undercrown R	235	219	-7
MP5 Undercrown F	235	216	-9
MP6 Skirt	160	157	-2
MP7 ALFIN ATS	320	316	-1
MAX		417	

Table 7.6 – CFD3D new tool tuning T_{wall} loop 2

For the sake of simplicity in figure 7.9, 7.10, and 7.11 are showed the obtained thermal map, only for case 3), in which the qualitative distribution shows the injection points. In all these simulations, the starting HTC's family is the one derived from the GTP calibration procedure.

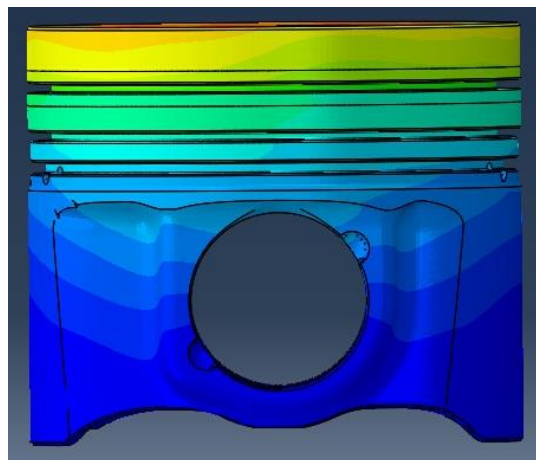


Figure 7.9 – Thermal map CFD3D new tool front

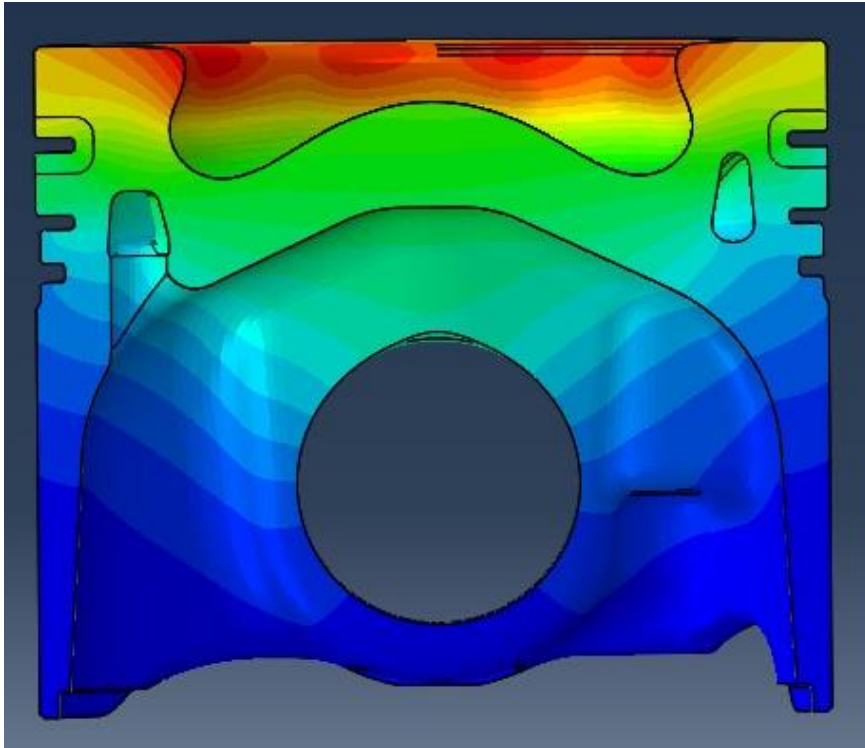


Figure 7.10 – Thermal map CFD3D new tool front section

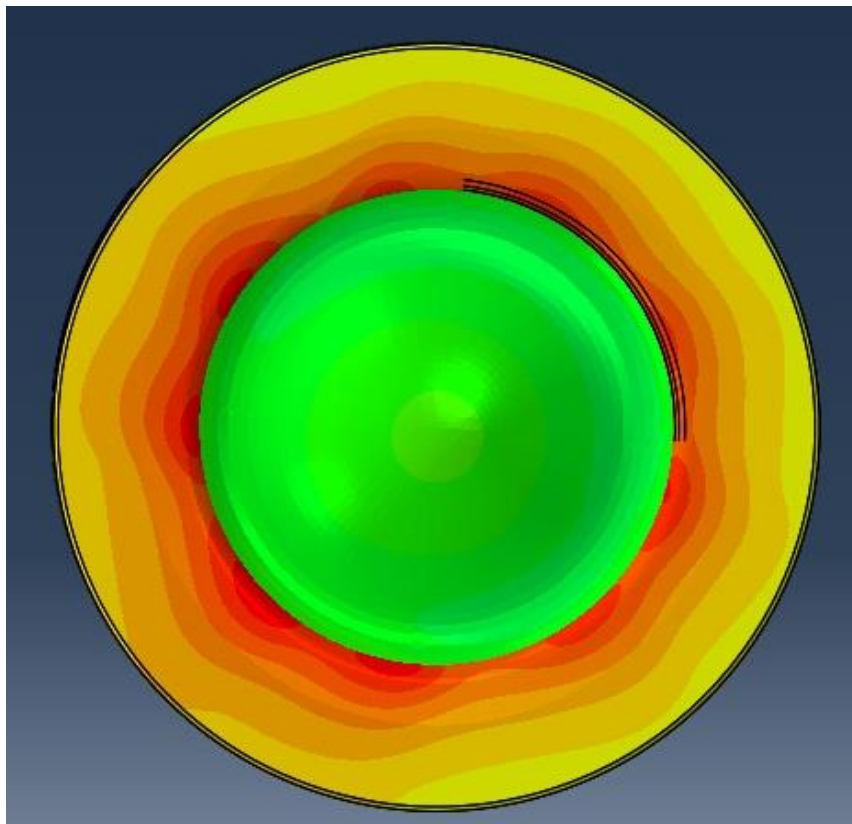


Figure 7.11 – Thermal map CFD3D new tool crown

7.4 FINAL COMPARISON

To compare the two procedures in figure 7.12 are shown the results sensor by sensor of the temperature value. The red bars represent the experimental telemetry value, the green ones represent the new procedure with the new tool, and in particular, the case 3), the yellow ones represent the results obtained with the actual method. It can be seen that the results are closer to each other and comparable. In the end, the main difference is how these results are obtained, because the green ones are obtained with a faster and more reliable procedure that requires fewer steps and especially less tuning procedure.

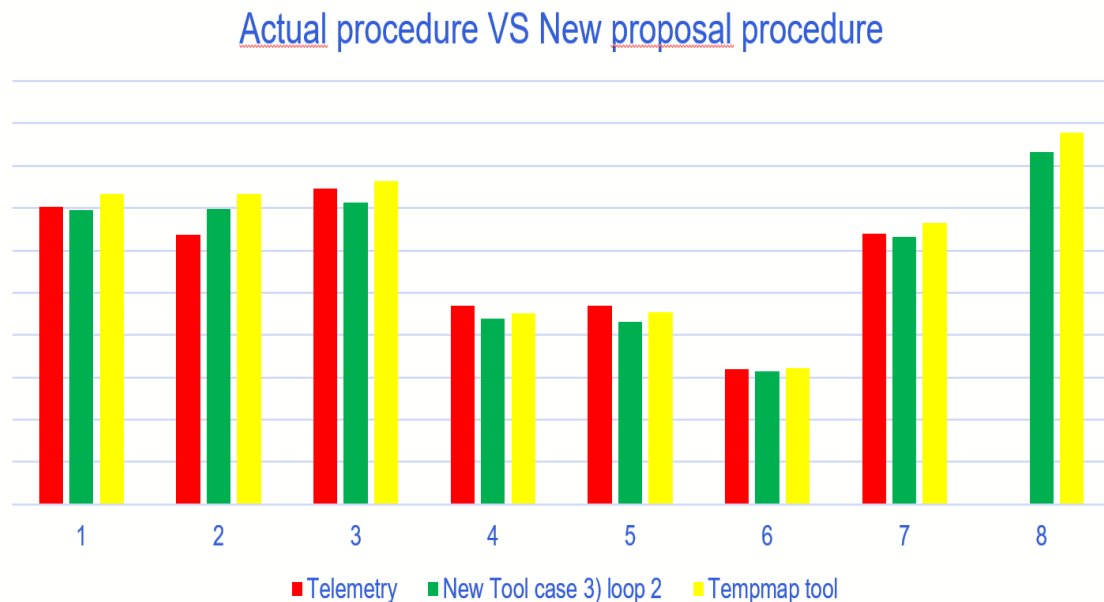


Figure 7.12 – Procedures results comparison

Another comparison is made concerning the different cases for the T_{wall} choice using the new tool. This is done to show the T_{wall} sensitivity, and from figure 7.13, it is even clearer that the first part of the actual procedure is not necessary; the green and the yellow bars are closer to the experimental value. The blue bars are the results obtained using the same approach of the actual procedure, and so with a thermal map coming from a previous GTP calibration; the yellow ones are the result considering a constant T_{wall} while the green ones are the result obtained with the thermal map coming from an earlier loop.

Twall sensitivity

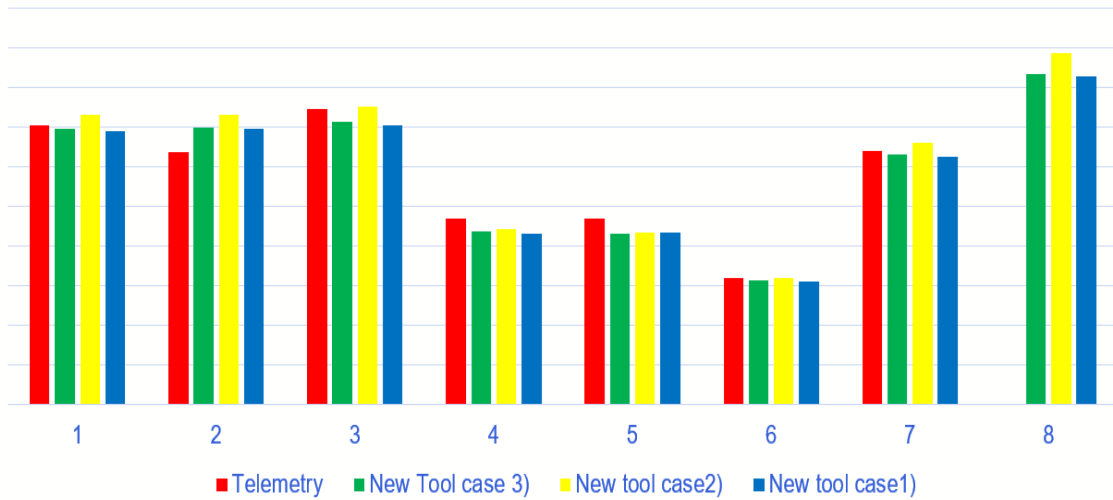


Figure 7.13 – Twall sensitivity

The last comparison is made considering three different calibrations:

1. GTP tuning of the actual procedure (Blue bars).
2. CFD3D with an internal tool of the actual procedure (Yellow bars).
3. CFD3D with the new tool of the new proposal procedure with case 3) (Green bars).

The red bars are the experimental values, and as shown in figure 7.14, the yellow calibration is less accurate, while the other two are closer to the red bars.

Final comparison

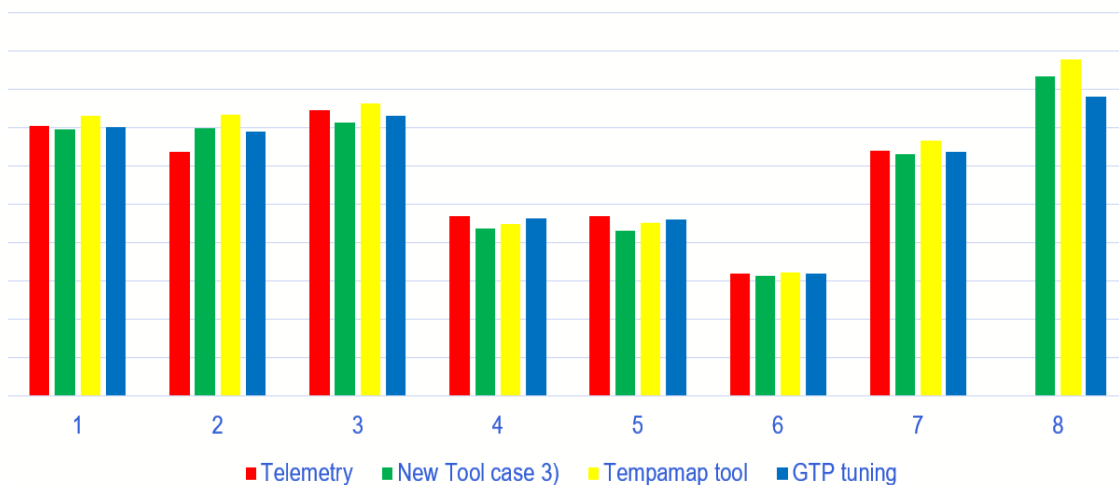


Figure 7.14 – Final comparison

7.5 THERMAL BALANCE ANALYSIS

To understand better the factor that affects most the calibration, a thermal balance analysis was carried on. This analysis calculates the percentage of heat dissipated region by region, considering the SOH [W], and the entering Q [W]. Once the percentages are calculated for each region, the results are compared with those shown in table 2.1, which are the ones found in [2] from the supplier Mahle. The results of this analysis are shown here below in table 7.7.

	GT-Power Tuning	CFD New Tool case 1)	CFD New Tool case 3)	CFD New Tool case 2)	Mahle reference
	[%]	[%]	[%]	[%]	[%]
Oil Gallery	49	50	49	50	40-50 %
Ring Pack	19	19	19	19	25-45 %
Skirt	22	22	22	22	5-10 %
Undercrown	12	11	11	11	5-15 %
Pinboss	0	0	0	0	0-10 %

Table 7.7 – Thermal balance analysis

The analyzed cases are:

1. GT-Power tuning of the actual procedure.
2. CFD new tool with GTP thermal map case 1).
3. CFD new tool with constant T_{wall} case 2).
4. CFD new tool loop 2 with the thermal map obtained from loop 1 case 3).

In all the cases, the unbalance is present in the ring pack and the skirt regions. The ring pack region dissipates less heat with respect Mahle indications, and this could be generated by:

- ❖ HTC's of that region are too low compared with the ones of the other regions.
- ❖ This kind of analysis does not consider the interaction with the liner and the friction generated in this zone.

The first point is related to the starting HTC's family choice that has to be improved and studied deeply for sure. The second one instead is related to the approximation done in the analysis, and in the model that does not consider these

interactions that are fundamental for the heat exchange process. In the skirt region, the situation is the opposite, because this region is dissipating twice with respect to what indicated by the supplier. Also, in this case, the problem is probably related to the HTC's choice that are higher with respect to what happens in reality.

8 INLINE 6 CYLINDER STEEL PISTON CASE STUDY

The second case study was performed on an inline six cylinders Diesel engine steel piston. This piston has a stepped bowl geometry, and because it is made of steel, the calibration procedure is more laborious with respect to an Al-alloy one. It has to be said that the CFD3D BCs have never been used on a steel piston in the company, and that the actual procedure was developed for Al-Alloy gasoline engine pistons. In figure 8.1 is shown the FEM mesh of the piston while in table 8.1 are reported the experimental temperature values acquired with Templugs.

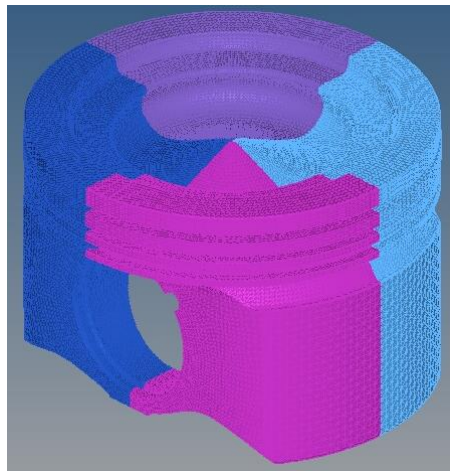


Figure 8.1 – Piston FEM mesh

NODE #	POSITION	TEMPLUG
[-]	[-]	[°C]
1	BOWL CENTER	425
2	TS / EXHAUST (PISTON CROWN)	362
3	TS - TOP LAND	368
4	TS - OIL GALLERY	257
5	REAR - BOWL RIM (EDGE 2)	406
6	TS - 2nd LAND	236
7	TS - BOWL RIM (EDGE 2)	385
8	ATS - OIL GALLERY	295
9	ATS - TOP LAND	428
10	ATS - BOWL RIM (EDGE 2)	431
11	ATS - 2nd LAND	258
12	REAR 30° - BOWL RIM (EDGE 2)	396
13	FRONT 30° - BOWL RIM (EDGE 2)	421
14	FRONT - BOWL RIM (EDGE 2)	405

Table 8.1 – Templugs experimental values

Before starting to analyze the different results obtained by the tuning procedures, it has to highlight two considerations:

- ❖ The first one regarding a discrepancy between CFD3D analysis and Templugs data, in fact, the first sensor that was put in the bowl center has acquired a temperature equal to 425°C as showed in table 8.1, while in the CFD3D analysis that zone has much lower Qfluxes values and so lower temperatures as shown in figure 8.2. The problem could depend on one hand by the fact that in this region are present turbulences, while on the other hand, the CFD3D analysis could have errors related to the spray penetration.
- ❖ The second one regards the fact that the GTP BCs were obtained with initial conditions slightly different with respect to the CFD3D ones, so the heat values to calculate the scaling coefficient were modified, basing on internal experience, to match the initial conditions.

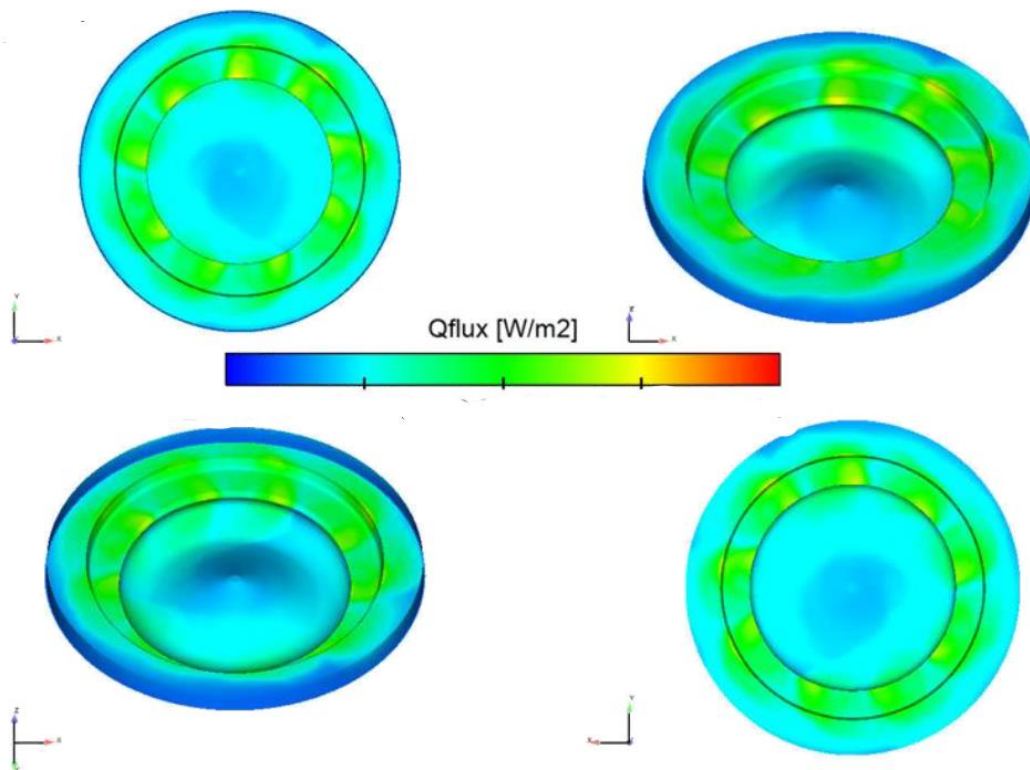


Figure 8.2 – CFD3D Qfluxes distribution

8.1 GT-POWER TUNING

The GT-Power tuning was performed exactly as in the previous case, following the actual procedure. In this case, the Qfluxes redistribution procedure is more difficult because the geometry is more complex, and the area of the FEM model is different with respect to the GTP one. At the end of this procedure, the first loop is performed, and the results are showed in table 8.2.

NODE #	POSITION	TEMPLUG	GTP 1st Loop	
			FEA Temperature	Difference vs. Templug
[-]	[-]	[°C]	[°C]	[°C]
1	BOWL CENTER	425	356	-69
2	TS / EXHAUST (PISTON CROWN)	362	344	-18
3	TS - TOP LAND	368	334	-34
4	TS - OIL GALLERY	257	276	20
5	REAR - BOWL RIM (EDGE 2)	406	390	-16
6	TS - 2nd LAND	236	238	2
7	TS - BOWL RIM (EDGE 2)	385	377	-8
8	ATS - OIL GALLERY	295	277	-18
9	ATS - TOP LAND	428	339	-88
10	ATS - BOWL RIM (EDGE 2)	431	378	-53
11	ATS - 2nd LAND	258	240	-18
12	REAR 30° - BOWL RIM (EDGE 2)	396	391	-5
13	FRONT 30° - BOWL RIM (EDGE 2)	421	374	-46
14	FRONT - BOWL RIM (EDGE 2)	405	378	-26

Table 8.2 – GTP tuning first loop

It can be seen that the temperature differences are higher with respect to the Al-alloy case, which confirms that it is harder to find a proper HTC's starting family for a steel piston. The first row is highlighted in red due to the consideration done in chapter 8. At this point, the HTCs were changed, and the tuning procedure was performed to match the experimental values. The final results of this tuning procedure are shown in table 8.3.

NODE #	POSITION	TEMPLUG	GTP Final Loop	
			FEA Temperature	Difference vs. Templug
[-]	[-]	[°C]	[°C]	[°C]
1	BOWL CENTER	425	429	4
2	TS / EXHAUST (PISTON CROWN)	362	360	-2
3	TS - TOP LAND	368	360	-8
4	TS - OIL GALLERY	257	288	31
5	REAR - BOWL RIM (EDGE 2)	406	398	-8
6	TS - 2nd LAND	236	245	10
7	TS - BOWL RIM (EDGE 2)	385	385	0
8	ATS - OIL GALLERY	295	310	14
9	ATS - TOP LAND	428	388	-39
10	ATS - BOWL RIM (EDGE 2)	431	420	-11
11	ATS - 2nd LAND	258	267	9
12	REAR 30° - BOWL RIM (EDGE 2)	396	392	-4
13	FRONT 30° - BOWL RIM (EDGE 2)	421	422	1
14	FRONT - BOWL RIM (EDGE 2)	405	409	5

Table 8.3 – GTP tuning final loop

In this calibration, the more significant differences are found in sensor 4 inside the oil gallery and the sensor 9 in the top land, and for both is higher than 30°C. For all the other sensors, the temperature differences are less than 15°C; the maximum temperature is equal to 499°C. In figure 8.3, 8.4, and 8.5 are showed the obtained thermal map.

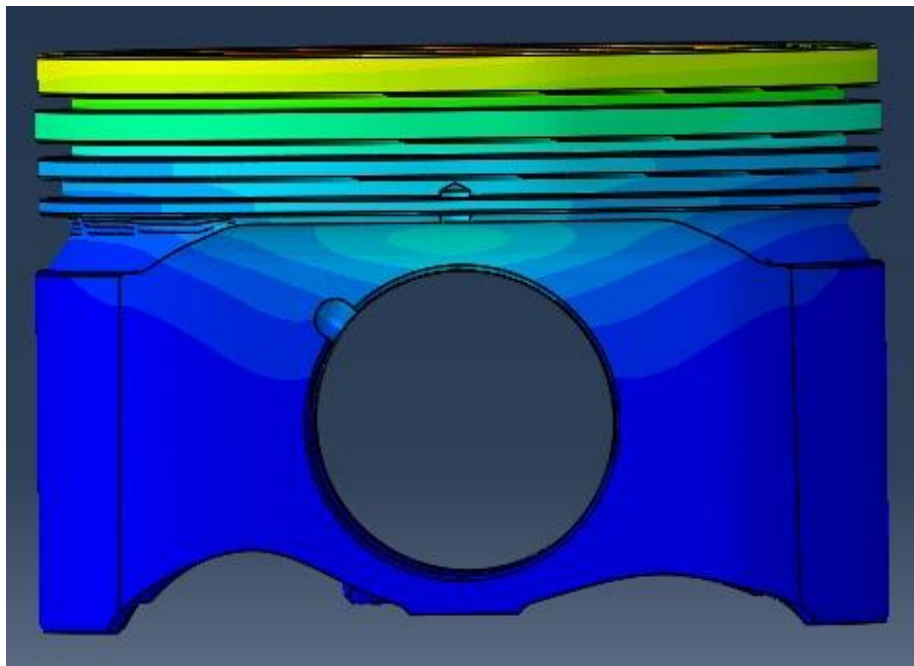


Figure 8.3 – Thermal map GTP front

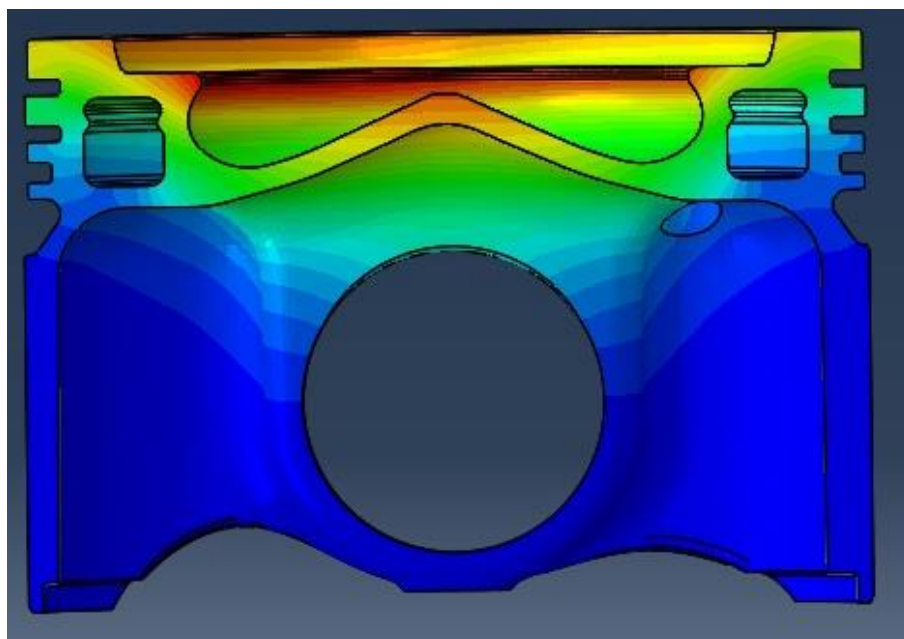


Figure 8.4 – Thermal map GTP front section

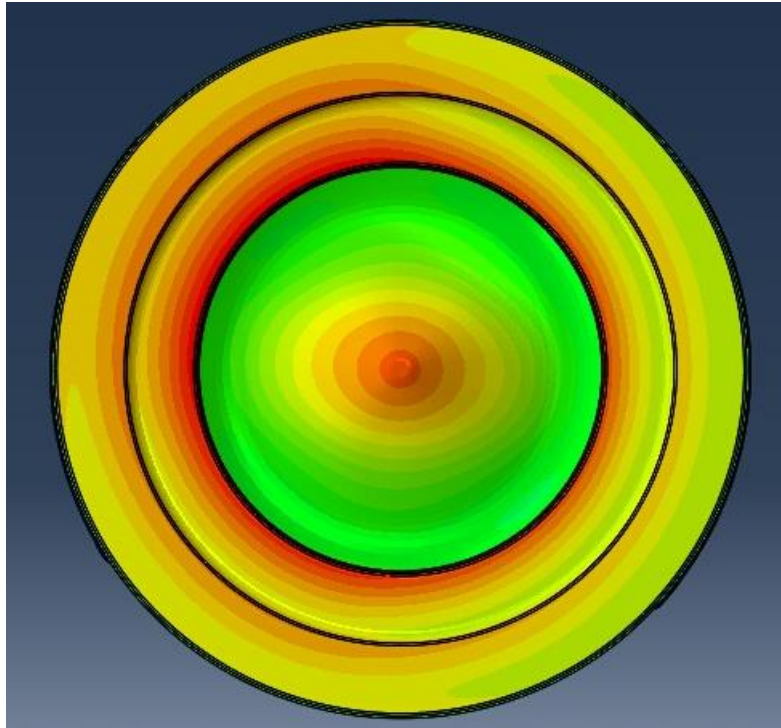


Figure 8.5 – Thermal map GTP crown

8.2 CFD3D TUNING: ACTUAL PROCEDURE

This is the first time that the actual procedure based on CFD3D BCs is applied to a steel piston, but the aim is the same as the previous case, so to obtain a more realistic thermal map with visible injection points. In table 8.4 are showed the results obtained with the actual procedure previously described.

NODE #	POSITION	TEMLUG	CFD3D Standrad Tuning	
			FEA Temperature	Difference vs. Templug
[-]	[-]	[°C]	[°C]	[°C]
1	BOWL CENTER	425	355	-70
2	TS / EXHAUST (PISTON CROWN)	362	429	67
3	TS - TOP LAND	368	421	53
4	TS - OIL GALLERY	257	322	66
5	REAR - BOWL RIM (EDGE 2)	406	445	39
6	TS - 2nd LAND	236	278	43
7	TS - BOWL RIM (EDGE 2)	385	474	89
8	ATS - OIL GALLERY	295	320	25
9	ATS - TOP LAND	428	430	3
10	ATS - BOWL RIM (EDGE 2)	431	447	16
11	ATS - 2nd LAND	258	289	31
12	REAR 30° - BOWL RIM (EDGE 2)	396	438	42
13	FRONT 30° - BOWL RIM (EDGE 2)	421	474	54
14	FRONT - BOWL RIM (EDGE 2)	405	443	39

Table 8.4 – CFD3D actual procedure tuning

As reported in the table, this calibration didn't lead to accurate results; the temperature differences are higher with respect to the Al-alloy case and greater than 40°C in the majority of the sensors. Moreover, the maximum temperature is equal to 615°C. It is clear that another tuning procedure is needed, changing the HTC's to obtain more reliable results. In figures 8.6, 8.7, and 8.8 are shown the thermal map. In all these simulations, the starting HTC's family is the one derived from the GTP calibration procedure.

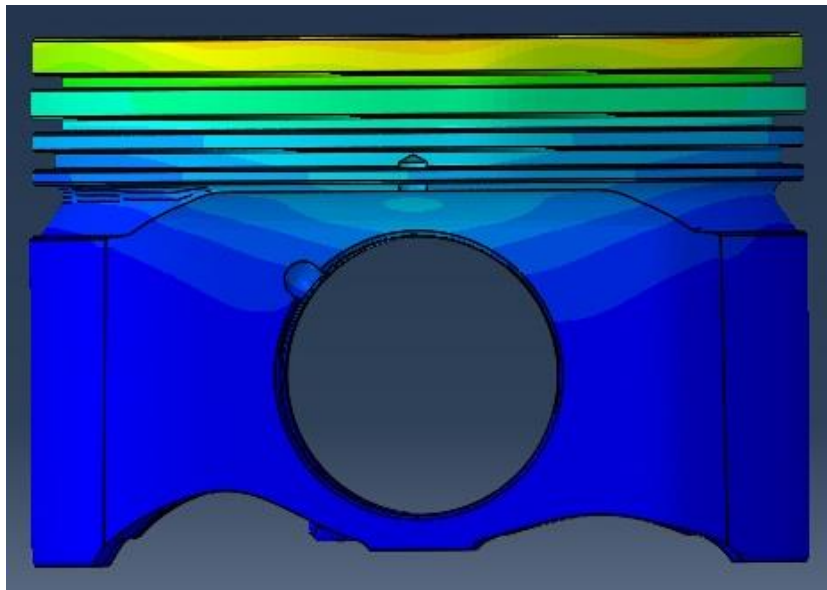


Figure 8.6 – Thermal map CFD front

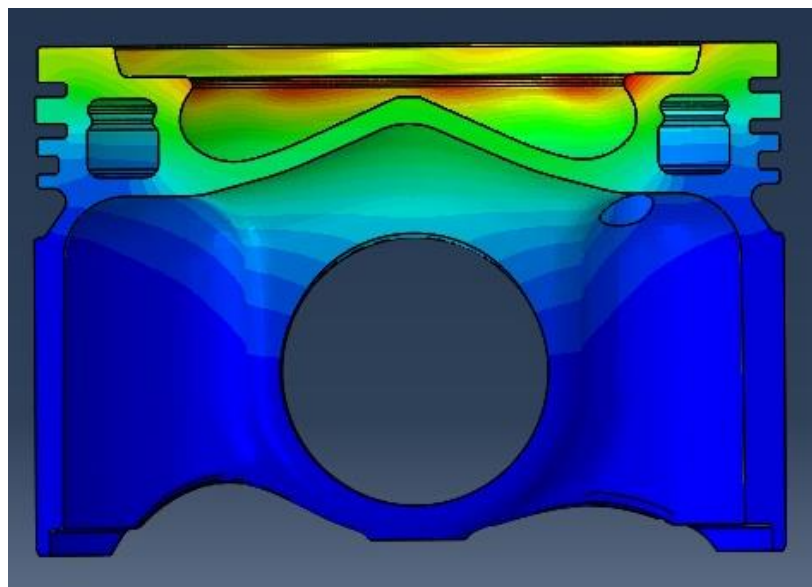


Figure 8.7 – Thermal map CFD front section

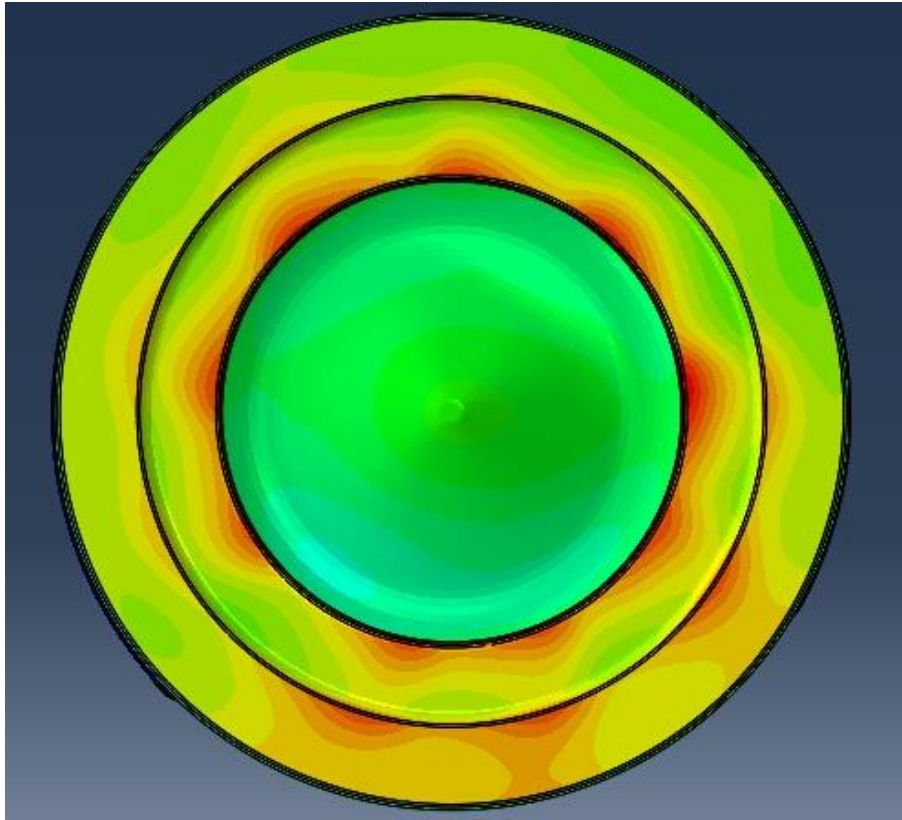


Figure 8.8 – Thermal map CFD front crown

8.3 NEW TOOL TUNING

The new procedure and the new tool were applied as was done for the first case study, but in this case, five different cases with different T_{wall} were analyzed:

1. Constant CFD3D T_{wall} .
2. Variable CFD3D T_{wall} .
3. Constant GT-Power T_{wall} .
4. Variable GT-Power T_{wall} . (Table 8.3)
5. T_{wall} taken from the previous loop. (case 2)

The case 1) results are shown in table 8.5 and, also in this case, it can be seen that the temperature differences are high, and in most of the cases higher than 40°C ; moreover, the maximum temperature is equal to 693°C that is much higher with respect to the current limit imposed by the company equal to 490°C .

NODE #	POSITION	TEMPUG	New Tool CFD Twall Constant	
			FEA Temperature	Difference vs. Tempug
			[°C]	[°C]
1	BOWL CENTER	425	338	-87
2	TS / EXHAUST (PISTON CROWN)	362	418	57
3	TS - TOP LAND	368	417	49
4	TS - OIL GALLERY	257	320	63
5	REAR - BOWL RIM (EDGE 2)	406	529	123
6	TS - 2nd LAND	236	278	43
7	TS - BOWL RIM (EDGE 2)	385	465	80
8	ATS - OIL GALLERY	295	323	28
9	ATS - TOP LAND	428	511	84
10	ATS - BOWL RIM (EDGE 2)	431	502	71
11	ATS - 2nd LAND	258	329	71
12	REAR 30° - BOWL RIM (EDGE 2)	396	488	92
13	FRONT 30° - BOWL RIM (EDGE 2)	421	485	65
14	FRONT - BOWL RIM (EDGE 2)	405	480	76

Table 8.5 – CFD3D new procedure tuning constant CFD Twall

Also, in case 2), the results were not so accurate, and the differences were higher than 40°C, moreover, the maximum temperature is equal to 657°C. Here below in table 8.6, the obtained results are shown.

NODE #	POSITION	TEMPUG	New Tool CFD Twall Not Constant	
			FEA Temperature	Difference vs. Tempug
			[°C]	[°C]
1	BOWL CENTER	425	306	-119
2	TS / EXHAUST (PISTON CROWN)	362	426	64
3	TS - TOP LAND	368	429	60
4	TS - OIL GALLERY	257	321	64
5	REAR - BOWL RIM (EDGE 2)	406	513	107
6	TS - 2nd LAND	236	283	47
7	TS - BOWL RIM (EDGE 2)	385	458	73
8	ATS - OIL GALLERY	295	326	31
9	ATS - TOP LAND	428	517	89
10	ATS - BOWL RIM (EDGE 2)	431	496	65
11	ATS - 2nd LAND	258	331	73
12	REAR 30° - BOWL RIM (EDGE 2)	396	479	83
13	FRONT 30° - BOWL RIM (EDGE 2)	421	484	64
14	FRONT - BOWL RIM (EDGE 2)	405	476	72

Table 8.6 – CFD3D new procedure tuning not constant CFD Twall

For case 3), the results are shown in table 8.7, and as can be seen, the temperature differences are lower with respect to the previous case but always higher than 40°C. In this case, the maximum temperature is equal to 669°C.

NODE #	POSITION	TEMPLUG	New Tool GTP Twall Constant	
			FEA Temperature	Difference vs. Templug
[-]	[-]	[°C]	[°C]	[°C]
1	BOWL CENTER	425	319	-106
2	TS / EXHAUST (PISTON CROWN)	362	401	39
3	TS - TOP LAND	368	399	31
4	TS - OIL GALLERY	257	309	53
5	REAR - BOWL RIM (EDGE 2)	406	510	104
6	TS - 2nd LAND	236	269	34
7	TS - BOWL RIM (EDGE 2)	385	448	63
8	ATS - OIL GALLERY	295	311	16
9	ATS - TOP LAND	428	489	62
10	ATS - BOWL RIM (EDGE 2)	431	482	51
11	ATS - 2nd LAND	258	317	59
12	REAR 30° - BOWL RIM (EDGE 2)	396	471	75
13	FRONT 30° - BOWL RIM (EDGE 2)	421	465	45
14	FRONT - BOWL RIM (EDGE 2)	405	461	57

Table 8.7 – CFD3D new procedure tuning constant GTP Twall

In case 4), using a thermal map coming from the previous GTP calibration are obtained, the results showed in table 8.8. As can be seen, the differences are lower with respect to the previous cases, but also, in this case, at some point, the temperature differences are higher than 40°C. The maximum temperature is equal to 615°C.

NODE #	POSITION	TEMPLUG	New Tool GTP Twall Not Constant	
			FEA Temperature	Difference vs. Templug
[-]	[-]	[°C]	[°C]	[°C]
1	BOWL CENTER	425	289	-136
2	TS / EXHAUST (PISTON CROWN)	362	380	18
3	TS - TOP LAND	368	377	9
4	TS - OIL GALLERY	257	304	47
5	REAR - BOWL RIM (EDGE 2)	406	476	70
6	TS - 2nd LAND	236	258	22
7	TS - BOWL RIM (EDGE 2)	385	424	39
8	ATS - OIL GALLERY	295	296	1
9	ATS - TOP LAND	428	445	17
10	ATS - BOWL RIM (EDGE 2)	431	438	6
11	ATS - 2nd LAND	258	294	36
12	REAR 30° - BOWL RIM (EDGE 2)	396	444	48
13	FRONT 30° - BOWL RIM (EDGE 2)	421	419	-2
14	FRONT - BOWL RIM (EDGE 2)	405	423	19

Table 8.8 – CFD3D new procedure tuning not constant GTP Twall

The most reliable results are obtained following the new proposal procedure, and so using the thermal map coming from the first loop for the second loop Twall. In this case, the difference are closer to the ones of the case 4) but with the main difference that the maximum temperature is equal to 528°C. Also, this time the

results confirm that the new procedure leads to results comparable to that obtained with the actual procedure, but with fewer steps and calibrations. The results coming from this calibration are shown in table 8.9, while in figures 8.9, 8.10, and 8.11 are shown the obtained thermal map for one case because the qualitative distribution is similar in all the cases. In all these simulations, the starting HTC's family is the one derived from the GTP calibration procedure.

NODE #	POSITION	TEMPLUG	New Tool Loop 2	
			FEA Temperature	Difference vs. Templug
[-]	[-]	[°C]	[°C]	[°C]
1	BOWL CENTER	425	336	-89
2	TS / EXHAUST (PISTON CROWN)	362	337	-24
3	TS - TOP LAND	368	332	-36
4	TS - OIL GALLERY	257	286	30
5	REAR - BOWL RIM (EDGE 2)	406	419	13
6	TS - 2nd LAND	236	235	-1
7	TS - BOWL RIM (EDGE 2)	385	382	-3
8	ATS - OIL GALLERY	295	276	-20
9	ATS - TOP LAND	428	365	-62
10	ATS - BOWL RIM (EDGE 2)	431	384	-48
11	ATS - 2nd LAND	258	253	-5
12	REAR 30° - BOWL RIM (EDGE 2)	396	399	3
13	FRONT 30° - BOWL RIM (EDGE 2)	421	373	-48
14	FRONT - BOWL RIM (EDGE 2)	405	378	-27

Table 8.9 – CFD3D new procedure tuning T_{wall} from previous loop

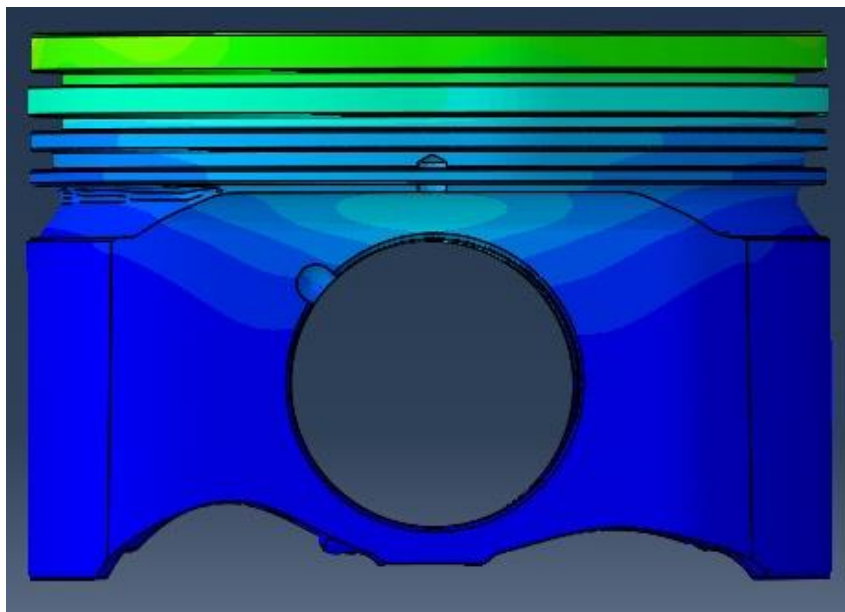


Figure 8.9 – Thermal map CFD new procedure front

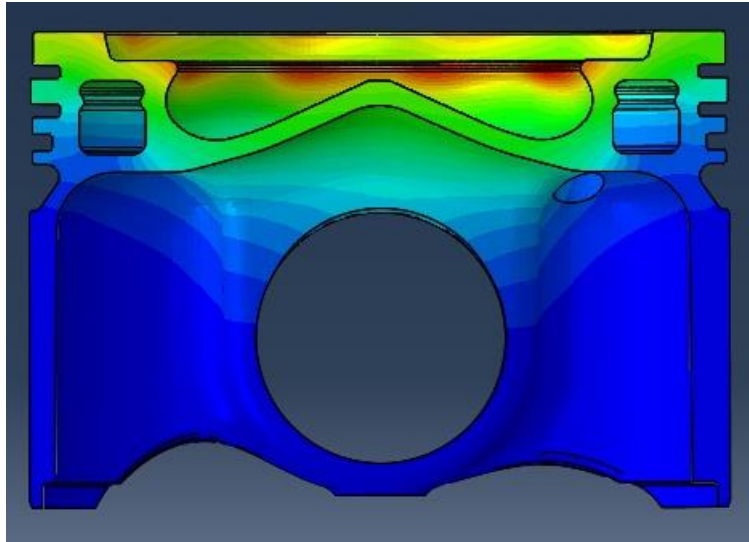


Figure 8.10 – Thermal map CFD new procedure front section

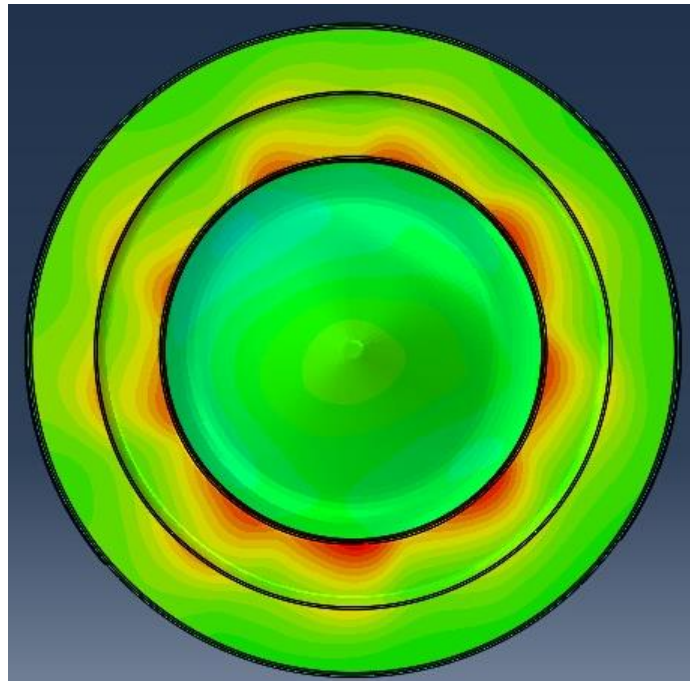


Figure 8.11 – Thermal map CFD new procedure crown

8.4 FINAL COMPARISON

In this chapter are compared the results obtained in different cases. The first comparison is shown in figure 8.12 and represents the differences between the actual procedure and the new one. In this graph, the red bars are the

experimental values, the green ones are the results obtained with the actual procedure while the yellow ones are obtained following the new procedure, and in particular, the case with T_{wall} taken from loop 1 (case 5). It can be seen that also if the results are not so accurate, the new procedure leads to values closer to the experimental one with respect to the actual procedure that overestimates the temperatures.

Actual procedure VS New proposal procedure

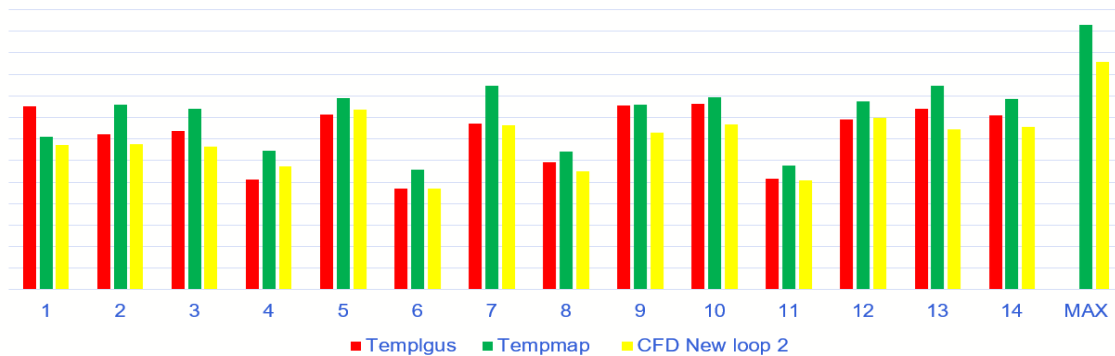


Figure 8.12 – Actual procedure VS New proposal procedure

The second comparison reported in figure 8.13, shown the differences between the T_{wall} choice. The reported cases are the same of the chapter 8.3, and in particular, the red bars are the experimental values, the green ones refer to case 1), the yellow ones to case 2), the blue ones to case 3), the black ones to case 4), and the purple one to the case 5). It is evident that the most reliable choice is the case 5) ones, so that demonstrates the correctness of the new proposal procedure.

T_{wall} choice

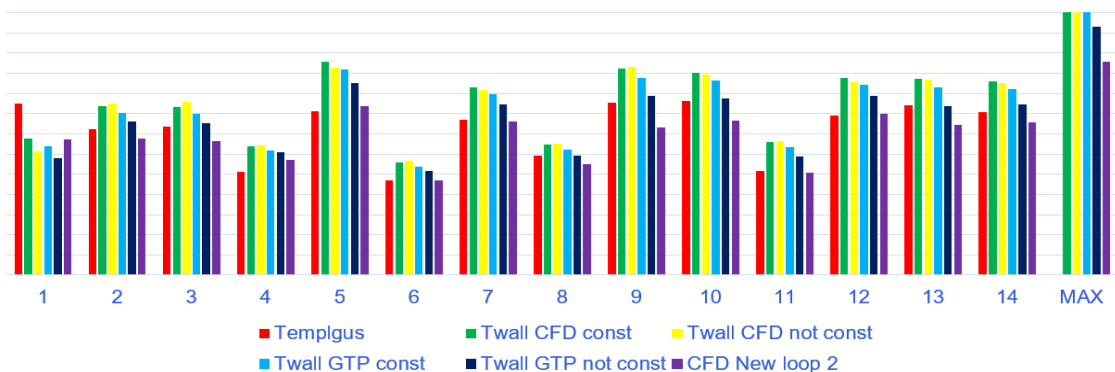


Figure 8.13 – T_{wall} choice

8.5 LOOP CONVERGENCY (ITERATIVE PROCEDURE)

Since the most reliable T_{wall} choice was the one coming from the use of the thermal map of the previous loop, it was carried out a convergency analysis to demonstrate the importance of the starting HTC's family. This analysis consists in to use the thermal map of the previous loop for the T_{wall} of the next one. Ten loops were made, and the results are shown in figure 8.14, where the red trace represents the experimental values.

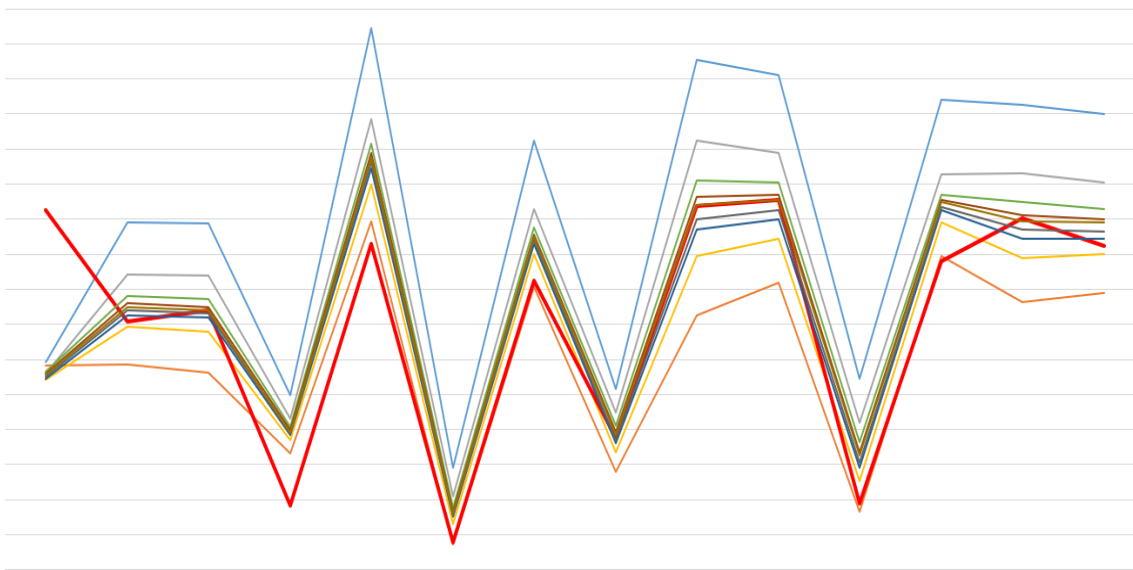


Figure 8.14 – Loop convergency

As can be seen, the curves are closer to the experimental curve going on with the loops, but in some points, there is not a convergence. These results strongly depend on the starting HTC's family, so the locations in which there is no convergence are the same that have shown less accurate results in the previously analyzed cases.

9 CONCLUSIONS

The whole first part of this thesis work composed of the literature investigation and the actual procedure analysis has led to a better understanding of the process and of the critical point on which it was needed a development. The data and the process cleaning procedure was of fundamental importance to arrive at the new proposal procedure. The actual method was developed for gasoline engines, so there was a need to create a new process for Diesel engines. With the new tool, the new procedure is more optimized, more accurate, and more reliable. The most important aspect of this work, shown in Table 6.1, is the reduction of tuning steps and operations that are often critical and so much time-consuming. Nowadays, it is fundamental to have a reliable process that, at the same time, is also fast and optimized, and the new procedure tries to follow that trend. It has to be said that as for all the new procedures, it can be further optimized and improved, but since the construction is highly straightforward, especially for what concerns the new tool structure, it will be easier to work on it. In conclusion, the whole work creates a new path for the steady-state thermal analysis on Diesel pistons that leads to accurate results for Al-alloys pistons but has to be improved for steel ones.

10 NEXT STEPS

Usually, the future works and next steps are presented together with the conclusion. In this case, the next steps have a fundamental importance, so it has been preferred to dedicate a separate chapter to them. The proposed next steps to improve the procedure are:

- ❖ Increase the accuracy of both CFD3D and GT-Power analyses will lead to more accurate results.
- ❖ For the CFD3D, the proposal concerns performing a more specific analysis for the piston because, at the moment, the analysis is done with particular focus on the combustion chamber. For example, the oil gallery is not considered, and it is evident that especially for Diesel engines, it has a high relevance to the heat transfer process.
- ❖ For the GT-Power, the next step could be to develop a 3D piston model, to have a better accuracy for what concerns heat fluxes, especially in cases in which the geometry is complex, as for the stepped one.
- ❖ The T_{wall} choice must be investigated deeply because, together with the HTC, it is the most critical factor for the convergence of the results.
- ❖ To obtain more predictable results must be developed a method to determine the starting HTCs family, and for this purpose could be used the semi-empirical correlations together with the IHCM and with the optimization algorithms.
- ❖ The new tool could be improved, optimized, and became more flexible.
- ❖ The whole procedure has to be improved to be also used with steel pistons, obtaining more accurate results.

REFERENCES

- [1] Incropera, F., DeWitt, D., Bergman, T., & Lavine, A. (2017). Principles of heat and mass transfer. Hoboken (New Jersey): J. Wiley & Sons.
- [2] M. GmbH(Ed). Pistons and engine testing. Wiesbaden: Vieweg+Teubner, 2011. isbn: 978-3-8348-1982-6.
- [3] N. S. Ottosen and H. Petersson. Introduction to the finite element method. New York: Prentice Hall, 1992. isbn: 0134738772; 9780134738772.
- [4] M. Gonera and O. Sandin. Thermal Analysis of a Diesel Piston and Cylinder Liner using the Inverse Heat Conduction Method. Chalmers Reproservice (Goteborg) 2015. ISSN 1652-8557
- [5] Esfahanian, V., Javaheri, A., & Ghaffarpour, M. (2006). Thermal analysis of an SI engine piston using different combustion boundary condition treatments. Applied Thermal Engineering, 26(2-3), 277-287. doi: 10.1016/j.applthermaleng.2005.05.002
- [6] Zheng, Q., Ma, C., & Zhang, J. (2013). Finite Element Analysis of the Piston Thermal Load in a Diesel Engine. Applied Mechanics And Materials, 459, 304-309. doi: 10.4028/www.scientific.net/amm.459.304
- [7] Lu, Y., Zhang, X., Xiang, P., & Dong, D. (2017). Analysis of thermal temperature fields and thermal stress under steady temperature field of diesel engine piston. Applied Thermal Engineering, 113, 796-812. doi: 10.1016/j.applthermaleng.2016.11.070
- [8] Barchenko, F., & Bakulin, V. (2017). Calculation of the Thermal Loading of the Cylinder-Piston Group of the Automobile Engine. Journal Of Engineering Physics And Thermophysics, 90(3), 657-664. doi: 10.1007/s10891-017-1613-y
- [9] Liu, X., Wang, Y., & Liu, W. (2017). Finite element analysis of thermo-mechanical conditions inside the piston of a diesel engine. Applied Thermal Engineering, 119, 312-318. doi: 10.1016/j.applthermaleng.2017.03.063
- [10] Chen, S., Meng, X., Guo, X., & Zhang, Y. (2014). Heat Transfer Boundary Conditions of Piston of Aviation Reciprocating Engine. Applied Mechanics And Materials, 602-605, 357-360. doi: 10.4028/www.scientific.net/amm.602-605.357

[11] Tiainen J., Kallio I., Leino A., Turunen R. (2004). Heat transfer study of a high power density diesel engine. ISSN: 0148-7191, e-ISSN: 2688-3627 DOI: <https://doi.org/10.4271/2004-01-2962>. Published October 25, 2004 by SAE International in United States

[12] Ismail, I., Emara, A., & Abdel Razek, E. (2016). Thermo Mechanical Analysis of a Direct Injection Heavy Duty Diesel Engine Piston Using FEA. Volume 6A: Energy. doi: 10.1115/imece2016-66160

[13] Seale, W., & Taylor, D. (1970). Spatial Variation of Heat Transfer to Pistons and Liners of Some Medium Speed Diesel Engines. Proceedings Of The Institution Of Mechanical Engineers, 185(1), 203-218. doi: 10.1243/pime_proc_1970_185_030_02

[14] Sharma, Subodh & Saini, Parveen & Samria, N.K.. (2015). Computational modeling of temperature field and heat transfer analysis for the piston of diesel engine with and without air cavity. Jordan Journal of Mechanical and Industrial Engineering. 9. 139-147.

[15] Ning, H., Dou, J., Huang, X., & Xie, Y. (2014). Thermal Load Simulation and Structure Improvement of High Speed Diesel Engine Piston. Applied Mechanics And Materials, 513-517, 2843-2846. doi: 10.4028/www.scientific.net/amm.513-517.2843

[16] Lu, X., Li, Q., Zhang, W., Guo, Y., He, T., & Zou, D. (2013). Thermal analysis on piston of marine diesel engine. Applied Thermal Engineering, 50(1), 168-176. doi: 10.1016/j.applthermaleng.2012.06.021

[17] He, T., Lu, X., & Guo, Y. (2011). Analysis of the Heat Transfer Coefficients on the Top of a Marine Diesel Piston Using the Inverse Heat Conduction Method. Advanced Materials Research, 291-294, 1657-1661. doi: 10.4028/www.scientific.net/amr.291-294.1657

[18] Madison, D., Miers, S., Barna, G., & Richerson, J. (2013). Comparison of Piston Temperature Measurement Methods: Templugs Versus Wireless Telemetry With Thermocouples. Journal Of Engineering For Gas Turbines And Power, 135(6). doi: 10.1115/1.4023493

[19] Ishibashi, A., Nakamura, M., & Muramatsu, H. (2014). Piston Temperature Measurement in Internal Combustion with Telemetric Method. SAE Technical Paper Series. doi: 10.4271/2014-32-0051

[20] Liu, Q., Ouyang, G., & Zhang, P. (2014). Three-Dimensional Finite Element Coupled Analysis of a Diesel Engine Piston. *Applied Mechanics And Materials*, 684, 347-353. doi: 10.4028/www.scientific.net/amm.684.347

[21] Ji, Y., Sun, P., & Zhao, S. (2014). Analysis of Temperature Field of High Speed Diesel Engine Parts and their Structural Optimization. *Applied Mechanics And Materials*, 490-491, 1003-1007. doi: 10.4028/www.scientific.net/amm.490-491.1003

ACKNOWLEDGMENTS

I would like to thank Prof.ssa Delprete for giving me this great opportunity, my tutor Alessandra Eleonora Gallinatti, my Engineering Manager Paolo Pagano, Alessandro Gallone, Vincenzo Pezza, and all the people of the Punch Torino S.p.a. for the support, availability, and kindness shown during these months of work. Finally, I would like to thank my family, fundamental and essential in everything I do and have done, and all my friends and those who have been part of this wonderful journey.